UNIVERSIDADE DE SÃO PAULO
INSTITUTO DE QUÍMICA
Programa de Pós-Graduação em Química

RAPHAEL DE ÁVILA NARCISO GOMES

Fotossensibilização em Modelos de Membrana e Células Neuronais

Versão corrigida da Dissertação defendida

São Paulo

Data do Depósito na SPG:

17 de março de 2021

RAPHAEL DE ÁVILA NARCISO GOMES

Photosensitization in Membrane Models and in Neuronal Cells

Dissertação apresentada ao Instituto de Química da Universidade de São Paulo para obtenção do Título de Mestre em Química

Orientador (a): Prof (a). Dr (a). Maurício da Silva Baptista

Collaboration: Professor Amalia Dolga

São Paulo
2021

Universidade de São Paulo
Instituto de Química

"Fotossensibilização em modelos de membrana e células neuronais"

RAPHAEL DE AVILA NARCISO GOMES

Dissertação de Mestrado submetida ao Instituto de Química da Universidade de São Paulo como parte dos requisitos necessários à obtenção do grau de Mestre em Ciências - no Programa de Química.

APROVADO(A) POR:

_____

Prof. Dr. Mauricio da Silva Baptista
(Orientador e Presidente)

_____

Profa. Dra. Cristina Kurachi
IFSC - USP

_____

Prof. Dr. Thiago Teixeira Tasso
UFMG

SÃO PAULO
30 de junho de 2021

Acknowledgments

I would like to acknowledge my advisor Mauricio, for the patience, effort, and care during these years, especially during these last couple of months. In addition, I would like to thank all the students and researchers of the lab, which helped me in so many situations, especially Dr. Helena Junqueira, Professor Dr. Thiago Tasso and Dr. Maidileyvis Castro Cabello. In addition, I am also grateful to Prof. Dr. Amalia Dolga (University of Groningen) and Prof. Dr. Martina Schmidt (Head Molecular Pharmacology - University of Groningen) for the support and teachings during my 5 months stay at University of Groningen. Also, would like to particularly thank the graduate and post-graduate students Inge, Shane and Dr. Marina Trombetta, which were good friends and helped me during my stay at Groningen.

I also would like to thank the professor Claudia Turro (University of Ohio) for providing the ruthenium complexes and professor Rosangela Itri (Physics Institute, Universidade de São Paulo) for allowing using her equipment and materials, especially for the analysis of the GUVs in chapter 2.

Further appreciate the Universidade de São Paulo for accepting my Master application and aid during the last few years. Likewise, this work would not be possible without the funding of Fundação de Amparo à Pesquisa do Estado de São Paulo (FAPESP, CEPID Redoxoma 2013/07937-8), Conselho Nacional de Desenvolvimento Científico e Tecnológico (CNPq), Coordenação de Aperfeiçoamento de Pessoal de Nível Superior (CAPES) and for scholarships. Finally, I aknowledge the University of Groningen (Erasmus+ ICM) for accepting and funding my Exchange program.

Finally, I would like to thank my friends from the University and from the high school for the laughs, drinks and help whenever I needed. Last, but not least I acknowledge my family for the support and motivation during these years, without them I would not be able to finish my thesis.

“Rapadura é doce, mas não é mole não.”

Autor desconhecido

“Há aqueles que lutam um dia, e por isso são muito bons;

há aqueles que lutam muitos dias, e por isso são muito bons;

há aqueles que lutam anos, e são melhores ainda.

Porém há aqueles que lutam toda a vida. Estes são os imprescindíveis.”

Bertold Brecht

RESUMO

Gomes, R.A.N **Photosensitization in Membrane Models and in Neuronal Cells**. 2021. 98p. Dissertação - Programa de Pós-Graduação em Química. Instituto de Química, Universidade de São Paulo, São Paulo.

A terapia fotodinâmica (TFD) está sendo amplamente estudada e testada para tratar diversos tipos de doenças, como câncer e doenças infecciosas. A TFD geralmente consiste no uso de fotossensibilizadores, oxigênio e luz para aumentar o estresse oxidativo em células e tecidos. Os fotossensibilizadores preferidos exibem: i) alto coeficiente de absorção na faixa visível do espectro luminoso; ii) alta eficiência de geração de estado excitado tripleto com energia adequada para permitir transferência de energia eficiente para formar oxigênio singlete; iii) propriedades físico-químicas e bioquímicas que permitam a interação com importantes alvos biológicos. Normalmente, compostos orgânicos, como porfirina ou derivados de sais fenotiazínicos, são usados como fotossensibilizadores (FS), mas complexos de rutênio também são compostos promissores para funcionar como fotossensibilizadores em TFD. Neste trabalho os efeitos fotodinâmicos dos complexos fotoativos de rutênio foram avaliados em modelos de membranas, ou seja, vesículas unilamelares pequenas (SUVs) e em vesículas unilamelares gigantes (GUVs), e em um modelo celular (Linha de Células Neuronais Hipocampais de Rato - HT22). A fototoxicidade dos complexos em células HT22 foi analisada, e o dano fotoquímico na célula e na mitocôndria foi observado por citometria de fluxo e microscopia. Os experimentos também foram projetados para comparar sua eficiência com um fenotiazínio eficiente (azul de 1,9-dimetilmetileno, DMMB). Os complexos de rutênio foram capazes de causar dano às membranas de GUVs e SUVs e a eficiência de dano não parece ter relação com a eficiência de geração de oxigênio singlete, mas sim com a ligação em membranas. Em células HT22, os complexos de rutênio foram capazes de danificar as mitocôndrias. Os danos não podem ser revertidos por agentes antioxidantes gerais. O LD50 foi calculado como sendo de 17 a 25 μM de 8.000 a 25.000 células, o que implica em concentrações intracelulares de ~ 80pM / célula. O DMMB também causa danos graves nas mitocôndrias, conforme indicado pela morfologia das mitocôndrias, coloração com MitoSox e peroxidação lipídica. O LD50 foi calculado em 30 a 35 e 40 nM para incubações com 5.000, 6.000 e 8.000 células, respectivamente, o que implica em concentrações intracelulares de ~ 2pM / célula. Foi observado que o DMMB é mais eficiente (~ 40 vezes) na diminuição de viabilidade celular (comparadas às concentrações intracelulares de PS no LD50), provavelmente devido à sua maior tendência para se ligar de forma mais eficiente às membranas. Esperamos ter maior eficiência em complexos de rutênio com mais ligantes lipofílicos.

Palavras-chave: Complexos de rutênio; DMMB; fotossensibilização; terapia fotodinâmica; membranas; células neuronais**.**

Abstract

Gomes, R.A.N **Photosensitization in Membrane Models and in Neuronal Cells**. 2021. 98p. Masters Thesis – Graduate Program in Chemistry. Instituto de Química, Universidade de São Paulo, São Paulo.

Photodynamic therapy (PDT) is being extensively studied and tested to treat different types of diseases, such as cancer, leishmaniosis, malaria, among others. PDT usually comprises the use of photosensitizers, oxygen and light to increase the oxidative stress in cells and tissues. Preferred photosensitizers display: i) high absorption coefficient in the visible range of the light spectra; ii) high efficiency of triplet excited state generation with energy suitable to allow efficient energy transfer to form singlet oxygen; iii) physical-chemical and biochemical properties that allow interaction with important biological targets. Usually organic compounds, such as porphyrin or phenothiazinium derivatives, are used as photosensitizers (PS), but ruthenium complexes are also promising compounds to function as PDT PS. In this work the photodynamic effects of ruthenium photoactive complexes were evaluated in membrane small unilamellar vesicles (SUVs) and giant unilamellar vesicles (GUVs) and in a cellular model (Mouse Hippocampal Neuronal Cell Line - HT22). The phototoxicity of the complexes in HT22 cells were analysed, and the photochemical damage in the cell and mitochondria was observed by flow cytometry and microscopy. Experiments were also designed to compare its efficiency with an efficient phenothiazinium (dimethyl-methylene blue DMMB). The ruthenium complexes were able to damage the membranes of GUVs and SUVs and the damage efficiency does not seem to be related to the efficiency of singlet oxygen generation, but to membrane bonding. In HT22 cells Ru complexes were able to damage mitochondria. Damage could not be reverted by general anti-oxidant agents. The LD50 were calculated to be from 17 to 25 μM from 8000 to 25000 cells, which implicates in intracellular concentrations of ~ 80pM/cell. DMMB also causes severe damage in mitochondria as indicated by mitochondria morphology, mitoSox staining, and lipid peroxidation. The LD50 were calculated to be 30 to 35 and 40 nM for incubations with 5000, 6000 and 8000 cells, respectively, which implicates in intracellular concentrations of ~2pM/cell. It is clear that DMMB is more efficient (~40 times) in terms of causing cell death (compared PS intracellular concentrations at the LD50), probably because for its higher tendency to bind more efficiently to membranes. We expect to have higher efficiency in Ru complexes with more lipophilic ligands.

Key-words: Ruthenium complexes; DMMB; photosensitization; photodynamic therapy; lipid membranes; neuronal cells.

Summary

Foreword

The general aim of the present study is to contribute to a better understanding of the photodynamic efficiency of ruthenium complexes in photodynamic therapy (PDT), by using Small Unilamellar Vesicles (SUVs) and Giant Unilamellar Vesicles (GUVs) as well as neuronal HT22 cells. We also aimed to compare the efficiency of photoinduced cell death and the intracellular target of Tris(bipyridine) ruthenium(II) ($Ru(bpy)_3Cl_2$) with that of Dimethyl Methylene Blue (DMMB) by using HT22 cells.

This dissertation is divided in four chapters: Chapter 1. Introduction about the state of the art related to photosensitized oxidation reactions, specially focusing in membrane oxidation and in induction of cell death; Chapter 2. We present and discuss results of the photochemical damage by ruthenium based photosensitizers in membrane models and in cells; Chapter 3. We present and discuss results of the photochemical damage by the phenothiazinium salt DMMB in mitochondria and cells.; Chapter 4. Conclusion and perspectives.

Chapter 1 – Introduction to Photosensitized oxidations

Photochemical Therapy Principles

Although there are many therapies for the treatment of cancer (surgery, chemotherapy and radiotherapy), alternative therapies are constantly being proposed in the area of oncology. Among the alternative therapies, photodynamic therapy (PDT) stands out, as a fairly recent clinical procedure in the treatment of cancer.[1–8] In photodynamic therapy (PDT) the combined action of irradiation with visible light and drugs that are photo-activated (photo-drugs, also called photosensitizers (PS)) are used to destroy tissues or pathogenic organisms, especially those that have rapid multiplication such as cancer.[9,10] Other diseases such as macular degeneration of the retina, psoriasis, fungal and bacterial infections, warts, which are also characterized by abnormal cell growth, are also being treated with PDT.[11–16]

The satisfactory result of a PDT treatment depends on a set of processes that are classically treated in different areas of specialization. In this context, as shown in Scheme 1, we can sub-divide the processes into three main areas that interface. They are: physical / photonic, chemical / biochemical and biological / medical. This classification is established between areas that use different theoretical-practical approaches. In addition, the tumor response to PDT treatment occurs at different time scales in each of these areas.

The main line of the project refers to photo-drugs that have been studied by us for some years and that have photophysical characteristics (high absorption in the spectral region above 600nm) and photochemical (efficient photogeneration of reactive species), making them promising for use in PDT.[17] This great efficiency allows the use of coherent sources of low energy or incoherent sources of irradiation, which reduces the cost and increases the range of treatments.

In the physical / photonic area, we will address the initial therapy process, which is the interaction of light with diseased tissue in the presence of the photo-drug. There is a great lack of models in this area that can predict the penetration and absorption of light by the sensitizer depending on the type of light, wavelength, drug concentration, type of tissue, etc. It is clear that the challenge is not small since it involves interactions between complex systems, but they are fundamental to the success of a given PDT treatment. Still in the area of photophysics, structural and image methods will be used to characterize the interaction of photo-drugs with membrane models, as well as to characterize the nanostructures we intend to synthesize.[18]

In the chemical / biochemical area, we will address the molecular aspects of this process, focusing in the mechanistic study of the photochemical and photobiological processes in membranes and complex systems such as organelles and cells in culture. Mechanistic studies relating photochemical efficiency and cyto-localization to the

efficiency and type of cell death (apoptosis or necrosis) are part of our current research objectives.

PDT is based on the photooxidation of biological matter. It is necessary to have a sensitizer, oxygen and light irradiation in the tissue to be treated. Reactive species are generated locally and cause cell death in tumor tissue.[19] Current research in the field of PDT focuses on the development of new drugs, the development of drug carrier systems and the understanding of the mechanisms of sensitization and cell death of drugs in vivo.[17,20,21]

Figure 1 shows a schematic of the photosensitization process. The absorption of light by the photosensitizer in the singlet fundamental state (S_0) leads to its passage to an excited singlet state (S_1), of high energy. This is quite unstable and can return to ground state due to loss of energy in the form of fluorescence or heat. On the other hand, a photosensitizer excited in the singlet state (S_1) can suffer an intersystem crossing, changing to an excited triplet state (T_1), of longer lifetime. This can return to the ground state by emitting phosphorescence or energy in the form of heat, or by transferring energy to molecular oxygen. Alternatively, the photosensitizer in the triplet excited state can also transfer electrons to a substrate. The reaction with biomolecules, through the transfer of electrons to form radicals, and subsequent reaction with oxygen, results in the production of ROSs such as the superoxide radical anion, hydrogen peroxide and the hydroxyl radical (type I reactions). In turn, the transfer of energy to oxygen leads to

the formation of singlet oxygen, a very reactive species (type II reaction). The mechanisms of photochemical attack on biomolecules can be separated into two classes. In the TYPE I mechanism, light energy passes from excited molecules to biomolecules through electron transfer (radical mechanism) that culminates in direct damage to biomolecules or in the formation of active oxygen species, for example, superoxide radical. In the TYPE II mechanism, the excitation energy is transferred to molecular oxygen, resulting in the formation of singlet oxygen ($^1O_2$), which is extremely electrophilic, being able to cause damage to lipids, proteins and DNA.[22]

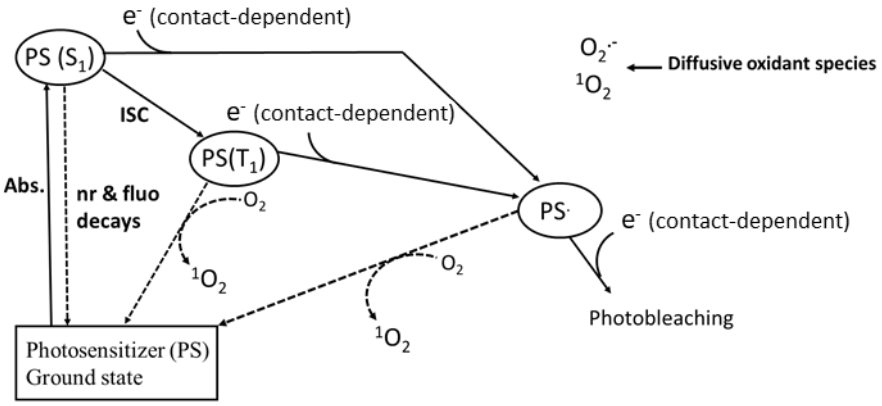

Figure 1. Scheme of the photosensitized oxidation reactions. The photosensitizer (PS) is a molecule capable to absorb light depending on its specific absorption spectra. Once excited, the PS transfers from its ground state PS(S0) to its singlet excited PS(S1) and triplet excited PS(T1) states by intersystem crossing (ISC). Both, PS(S1) and PS(T1) can react directly with biomolecules, like carbohydrates, lipids, proteins or nucleic acids, via Type I contact-dependent reaction, resulting in formation of radicals, like $PS^{\cdot}$, capable to initiate radical chain reactions. Otherwise, PS (T1) can react with molecular oxygen $^3O_2$, via the Type II reaction, generating singlet oxygen $^1O_2$. Both diffusive oxidant species as the excited state species are involved in the oxidative damage. Furthermore, the excited molecules can decay to the ground state by non-radioactive (nr) and fluorescence (fluo)decays.

Damage to membranes is of particular interest to the PDT process, since sensitizers tend to accumulate in cell and/or organelles membranes. Illumination of the membranes with sensitizer leads to cell damage and death.[23] In chemical terms, changes in phospholipids occur due to lipid peroxidation, which are reactions that start as a consequence of the formation of free radicals and singlet oxygen.[24] Once started, the process becomes autocatalytic, leading to the formation of hydroperoxides and secondary products.

The lipid peroxidation process can be summarized by three phases: Initiation, Propagation and Termination. Initiation occurs with the abstraction of a hydrogen atom from an unsaturated fatty acid (LH), leading to the formation of a lipid radical (L•). It undergoes the addition of an oxygen molecule forming the peroxyl radical (LOO•). It is able to react with another LH fatty acid, initiating a new oxidation chain that leads to the formation of lipid hydroperoxide (LOOH) and another lipid radical (L•). The propagation phase comprises the beginning of a new oxidation chain by the peroxyl radical (LOO•) and the decomposition of lipid hydroperoxides into other intermediate radicals.[25] In the case of the singlet oxygen-induced process, the formation of the initial hydroperoxide can be accompanied by internal cyclization and the formation of a second radical that can undergo oxygen attack, forming a cyclic hydropexil peroxide that leads to several carbonyl products[25].

The mechanism by which lipid oxidation cause irreversible membrane damage was described recently.[26] Irreversible membrane damage starts with the abstraction of a hydrogen from the double bond of an unsaturated fatty acid. This is a direct reaction with the triplet excited state of the photosensitizer. Subsequent formation of peroxyl and alkoxyl radicals favours the accumulation of lipid truncated aldehydes, which are the final responsible for opening membrane pores. The fact that the irreversible damage occurs after the reactions that require the contact between the excited state photosensitizer and the biological target, indicates that the damage can be confined within the nanometer location site of the PS.[27] Literature results indicate that membrane partition of the photosensitizer is the best predictive factor to explain efficiency of photodamage, indicating the important role of the so-called contact-dependent reaction (Figure 2). Usually, membrane partition is calculated by the proportion of PS localized in the membrane in relation to the amount dissolved in water, after a selected incubation time.

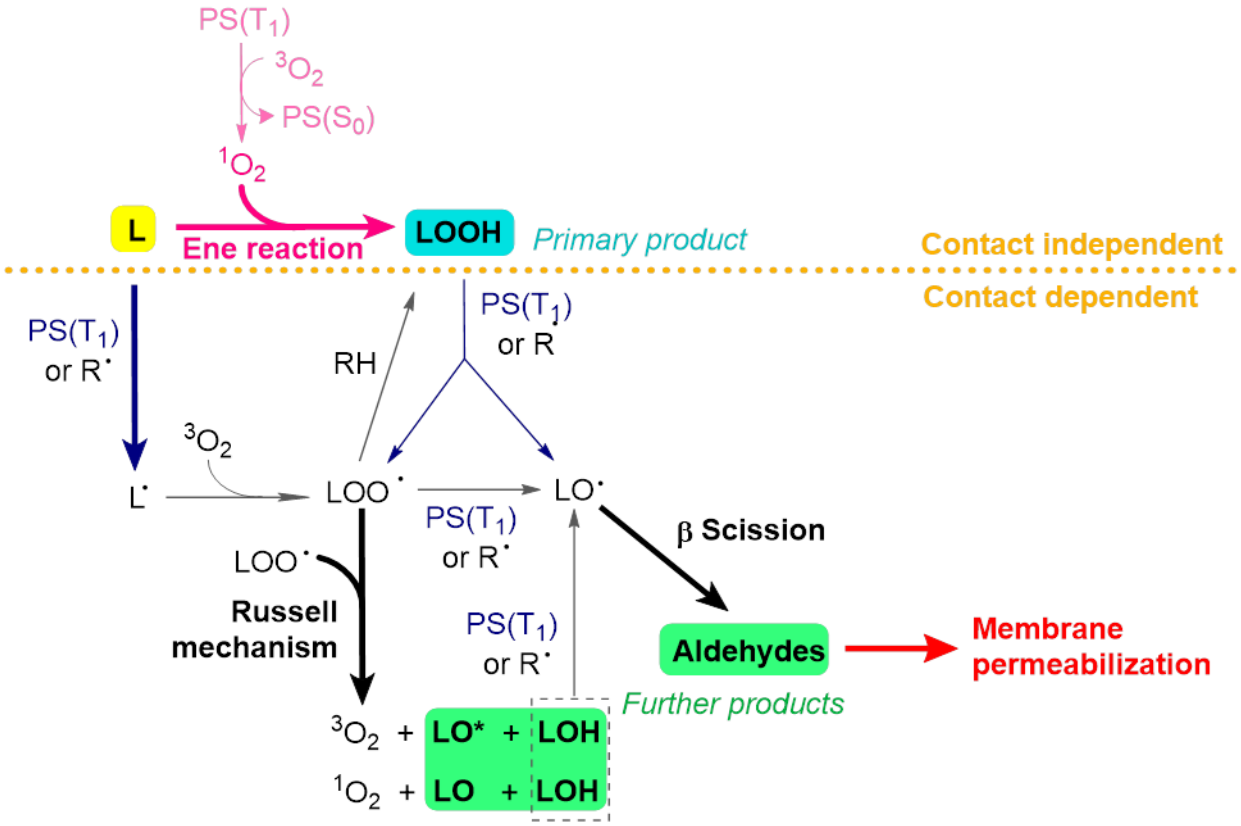

Figure 2. Type I and Type II photosensitization mechanisms, where BM is biomolecule, PS is photosensitizer. In the contact independent pathway (type II) no contact between the PS and the membrane is necessary. However, in the contact dependent pathway (type I), it can be seen that different products can be achieved, upon contact of the PS with the membrane, wherein these products can react with further biological targets, such as lipids, proteins, DNA. Adapted from Bacellar et al, 2018 [26]

There are several mechanisms of cell death, for example by necrosis or apoptosis and autophagy.[28,29] Necrosis is a mode of death associated with loss of homeostatic control, swelling and rupture of the cell membrane.[30] In apoptosis there is contraction of the cell, breakdown of the nuclear DNA, preventing its leakage and finally phagocytosis of the cell debris, without causing damage to neighboring structures.[31]

The mechanism of cell death caused by PDT is dependent on the photosensitizer, biological site of the photosensitizer, the cell and the treatment conditions employed, such as irradiance, time of photosensitization, medium etc.. Although the subject is still conjecture, it is known that $^1O_2$ damage, depending of the intracellular localization and concentration, has a tendency to induce cell death by apoptosis[32] while radicals derived from sensitizers have a tendency to induce death by necrosis.[33] The induction of damage in key organelles such as the mitochondria also favors apoptosis while the fission in the cytoplasmic membrane induces necrosis. A common point in all cases is that the cell's ATP level must be high for it to enter an apoptotic process.[32-33]

The apoptotic process may involve a so-called extrinsic signaling route, which involves activation of TNF receptors, formation of the Faz-FADD complex and activation of caspase-8, or the intrinsic route involves the release of cytochrome-c to the cytosol, oligomerization of Apaf-1 and activation of caspase-9. In the intrinsic pathway of apoptosis, the role of proteins in the BCL-2 family is undoubtedly important and can play antagonistic roles in inhibiting and activating apoptosis. These proteins are associated with the formation of pores in the internal mitochondrial membrane and the release of proteins in the cytosol. Although the oxidation of proteins of the BCL-2 family by singlet oxygen has already been described, the main pathways of activation of the apoptotic process by sensitizers used in PDT are still conjecture. There is no established

relationship between structure, cytolocalization and apoptotic activity, which is one of our research objectives in this project.

Most of the drugs that are being used in cancer treatments by PDT or that are in clinical tests in PDT are efficient generators of $^1O_2$ and the mechanism of action of these molecules depends on the presence of oxygen.[34,35] In fact, using the light emission measurement equipment at the NIR that was developed previously by the group, to measure the radioactive decay of singlet oxygen at 1270 nm, we obtained the efficiency of generating singlet oxygen from several photoactive molecules including phenothiazine dyes.[36]

In many cases, cutting the oxygen supply to the tumor, resulting from the treatment of PDT (destruction of the tumor vasculature), causes a decrease in its efficiency. Thus, one of the current research objectives in PDT is the development of sensitizers that directly and specifically destroy cellular organelles (e.g., mitochondria) of tumors and that act in the presence and absence of oxygen.[37]

The study of photochemical reactions at interfaces is an active area of research with implications in several fields: photography, energy conversion and PDT. Membranes and different interfaces can favor or disfavor various types of photochemical reactions by a supra-molecular organization effect, where the several reagents are positioned asymmetrically, directing the photophysical and photochemical properties of photoactive molecules.[38]

We used several supramolecular aggregates and structures to mimic interfaces with different characteristics. Each of these systems has its own characteristics. For example, vesicles consist of a lipid bilayer that separates an internal aqueous well from the external aqueous medium, reverse micelles are made up of a layer of surfactant that separates the internal aqueous well from the external organic medium, etc. The advantage of these systems is that their structural and physico-chemical properties can be varied precisely.[39]

Chapter 2 – Photochemical damage of Ruthenium Photosensitizers

2.1 Background

The damage to biological membranes is a critical step in defining the efficiency and the mechanism of cell death induced by a PDT protocol.[40] The strength of the interaction with membranes definitively affects the efficiency of a photosensitizer in damaging the membrane itself. Perhaps the most evident finding is the work in which a series of meso-substituted porphyrins containing 1 to 4 cationic groups on the periphery of the molecule were prepared. The amphiphilic PSs was shown to be several times more efficient at breaking through erythrocytes than the symmetrical ones.[41] The amphiphilic structure (molecular asymmetry in terms of polar and nonpolar regions) is clearly a structural feature that improves the efficiency of PSs in PDT, because it increases the ability of the PS to cross membranes and allows photo-reactions to occur in the membrane environment that has the highest concentration of oxygen and where the damage sites are located (unsaturation).

This example clearly shows the fundamental role of binding in membranes in the PDT efficiency. Therefore, understanding photosensitization processes is key to understand the efficiency of a PDT photosensitizer. Several models can be used to

study the effect of the photosensitized oxidation reactions on membranes: Giant Unilamellar Vesicles (GUVs) with observation through optical microscopy (OM), small unilamellar vesicles with observation by spectroscopic techniques.[39]

The first description of the use of the GUV technique with optical observation to understand biophysical damage in membranes was carried out by our group in collaboration with the group of prof. C. Marques ICS, Strasbourg, France and prof. Rosangela Itri, IFUSP. GUVs immersed in several photosensitization conditions were destroyed after a few minutes of irradiation. The membrane injury mechanism was attributed to the rupture of the lipid chain through the attack of triplet species of the photosensitizer as well as singlet oxygen to the double bond, with the formation of short chain amphiphiles.[42]

Data obtained by our and other groups indicate that the efficiency of the induction of the various mechanisms of cell death is critically dependent on the efficiency of a given drug to bind to intracellular membranes and organelles. Therefore, correlations of cell death and membrane damage are key to the development of novel PDT photosensitizers.[43]

Inorganic complexes offer the possibility of building multifunctional photosensitizers, since each central metal ligand can perform a specific function in the photosensitization process. Inorganic complexes can be covalently linked to biomolecules such as proteins and DNA, by fixing them to metal. This coordination

represents a key feature of the mechanism of action of cisplatin, one of the main leading anticancer drugs.[44] The transition metal complexes with photolabile ligands are capable of covalently joining biomolecules in a similar way to cisplatin, but only from irradiation with visible light. The requirement to use photons for their activation results in greater space-time selectivity regarding the tumor tissue in contrast to traditional medicines.[45] In addition, the transition metal complexes, which are activated by light, have been shown to be less toxic in the dark, and also to exhibiting a significant increase in cytotoxicity after irradiation.[46] Multiproposal complexes have been synthesized. These molecules can generate triplets and singlet oxygen and can also react by ligand exchange. In a series of molecules the ones that can do both of these mechanisms was shown to be more efficient[47] Nevertheless, there is no information in the scientific literature correlating membrane binding and damage with the photodynamic efficiency of inducing cell death.

In this chapter we aim to understand the mechanisms of photochemical damage of Ruthenium complexes in membrane models, such as Small Unilamelar Vesicles and Giant Unilamellar Vesicles and correlate with the efficiency of photoinduced cell death

2.2 Materials and Methods

The ruthenium photosensitizers were provided by the group of Professor Turro, (Ohio State University), a collaborator in this project. All aqueous solutions were

prepared with Mili-Q water. A buffer from tris(hydroxymethyl)aminomethane (Tris), pH = 8, was used in any moment when a buffered solution was necessary (“Buffer Tris”).

2.2.1 Photosensitizers

The ruthenium photosensitizers were the chloride complexes $[Ru(bpy)_3]Cl_2$, $[Ru(tpy)(ACN)_3]Cl_2$ and $[Ru(tpy)(5CNU)_3]Cl_2$ (figure 3), and the hexafluorophosphate complexes $[Ru(dqpy)(phen)(5CNU)][PF_6]_2$, $[Ru(dqpy)(phen)(ACN)][PF_6]_2$, $[Ru(dqpy)(dppn)(5CNU)][PF_6]_2$ and $[Ru(dqpy)(dppn)(ACN)][PF_6]_2$ (figure 4). These compounds were prepared by the group of prof. Claudia Turro (Ohio State University).

Table 1. Ligands names and respective structures

Ligand	**Structure**
2,2′-Bipyridine - BPY	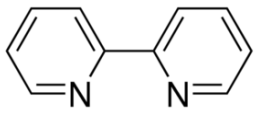
Terpyridine - TPY	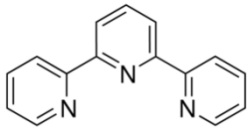
Acetonitrile - ACN	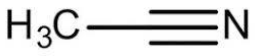

5-Cyanouracil - CNU	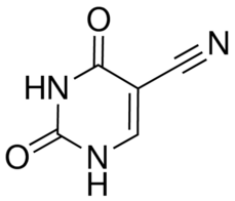
2,6-di(quinolin-2-yl)pyridine - DQPY	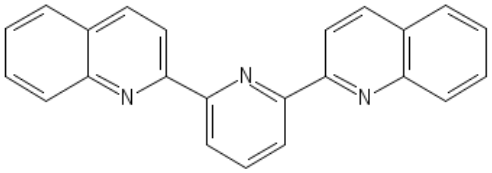
1,10-phenanthroline - Phen	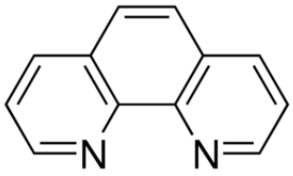
3,6-bis(2′-pyridyl)pyridazine - DPPN	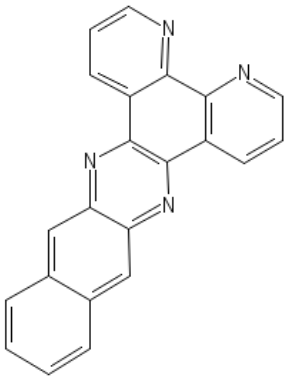

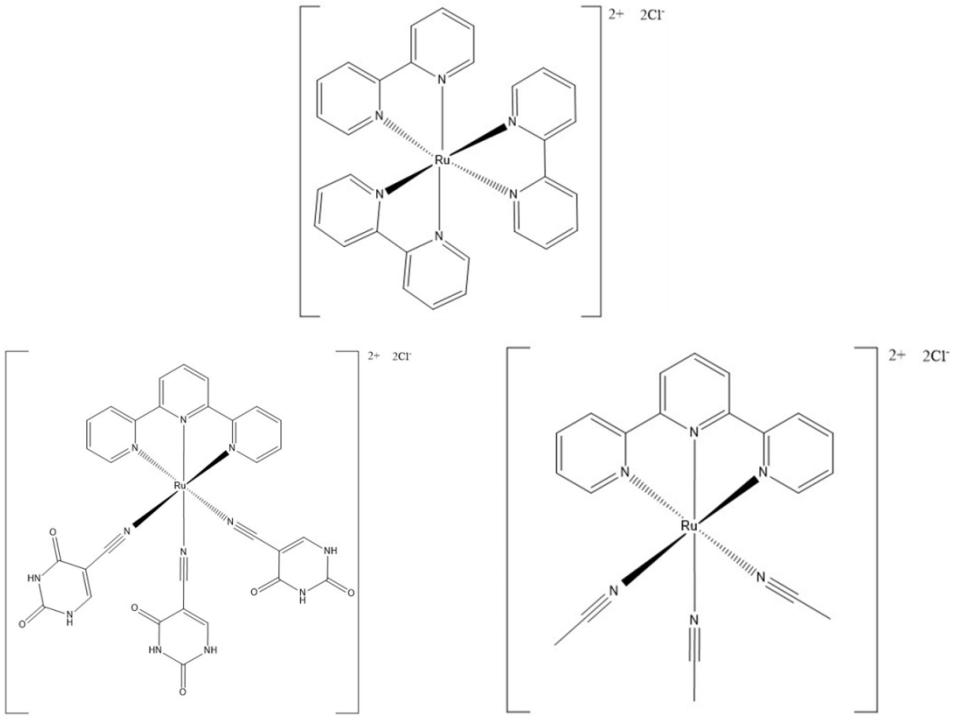

Figure 3. Ruthenium Chloride Complexes used in this work. Tris(bipyridine) ruthenium(II) chloride (superior), terpyridinetri(uracile) ruthenium(II) chloride (left) and terpyridinetri(acetonitrile) ruthenium(II) chloride (right).

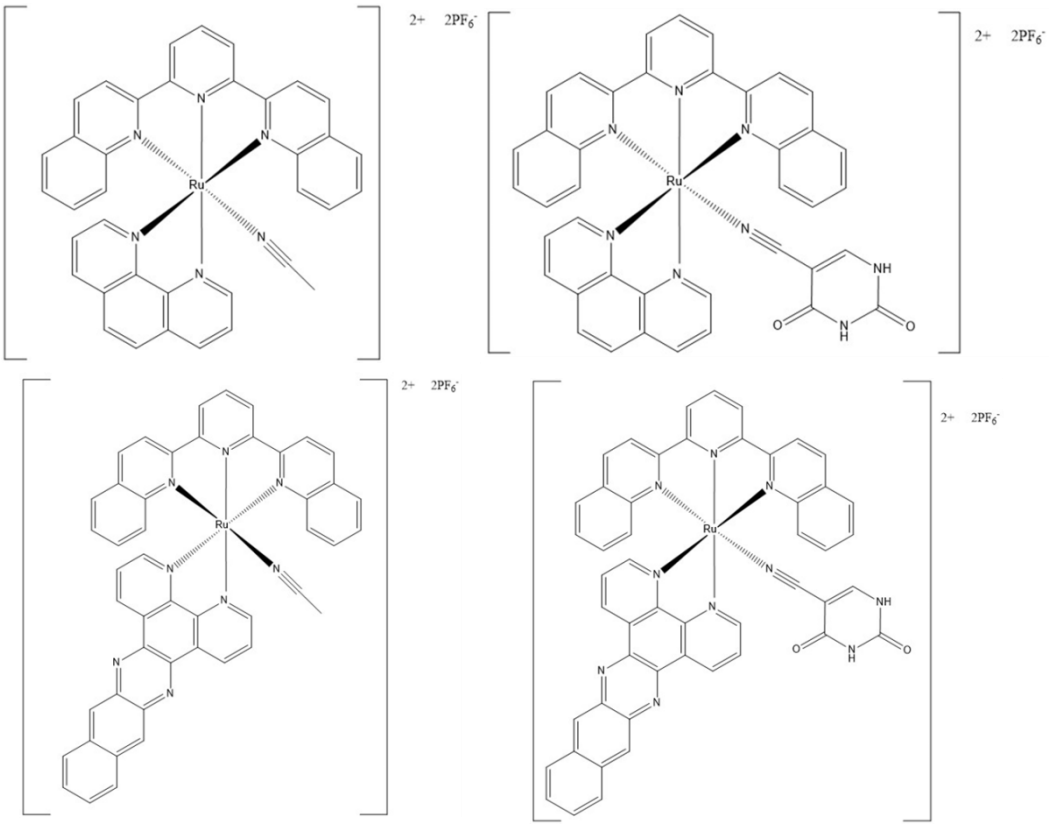

Figure 4. Ruthenium hexafluorophosphate complexes. Diquinolinylpyridinephenanthrolineacetonitrile ruthenium(II) hexafluorophosphate (superior right corner), diquinolinylpyridinephenanthrolineuracile ruthenium(II) hexafluorophosphate (superior left corner), diquinolinylpyridinedipyridylpyridazineacetontirile ruthenium(II) hexafluorophosphate (inferior right corner), diquinolinylpyridinedipyridylpyridazineuracile ruthenium(II) hexafluorophosphate (inferior left corner).

2.2.2 Photophysical Properties

Absorption spectra were recorded with a Shimadzu UV-1800 spectrophotometer in the range 200 nm to 800 nm. Molar absorptivity (ε_{max}) at the maximum absorption wavelength (λ_{max}) in each solvent was determined by measuring the absorption spectrum as a function of PS concentration (0.25 to 20 μM) and applying the Beer-

Lambert law. (table 2). It is important to note that the absorption spectra varies with the solvent, concentration of ions and pH.

Emission spectra were obtained with a Varian Cary 4 Cell Holder fluorometer. fluorescence efficiencies (n_f) were calculated by correlating the total area below the emission spectrum using a solution of the [$Ru(bpy)_3Cl_2$] complex as standard[48] (Table 2).

Singlet oxygen generation quantum yields (Φ_Δ) and $^1O_2$ lifetimes were determined by using a near-infrared time-resolved phosphorometer equipped with a Hamamatsu R55009 photomultiplier. A continuous laser (Nd: YAG, 532 nm) was used to pulse a color laser at a suitable wavelength (between 400 and 550 nm). The equipment was built in the laboratory and has been described in other publications.[49] Phosphorescence decay curves at 1270 nm were adjusted for a first order exponential decay for the determination of $^1O_2$ lifetime. For Φ_Δ measurements, the total area under the curve was analysed using a methylene blue solution or a [$Ru(bpy)_3Cl_2$] solution as standard in acetonitrile.[50]

2.2.3 Aggregations Trends (Attachment 1)

The aggregation trend of each PS was studied in different ionic forces, by comparing the absorption spectra of the PS solutions in water and in 3 M and 5 M NaCl solutions with the solutions in the pure solvent. The spectra were performed with a

Shimadzu UV-1800 spectrophotometer. Measurements were also made in PS solutions in 0.3 M NaCl solutions in Tris buffer, in the presence and absence of liposomes. To obtain a suspension of liposomes, lipid films (15 mg) were prepared in test tubes by evaporating a lipid solution in chloroform. The films were hydrated with 0.5 mL of the 0.3 M NaCl solution in Tris buffer, and suspended by vortexing for a few minutes. To subtract the contribution of spreading the absorption spectrum of the studied liposome suspensions, a blank comprising the same amount of liposomes (but without PS) was employed. Absorption spectra were collected between 0 and 60 min of incubation[51] The aggregation trend was analysed by the ratio between the absorbance values between the absorbance peaks of the monomer and the aggregate (Monomer / Aggregate ratio).

2.2.4 Membrane Association

Liposomes suspensions were prepared using 30 mg of lipids (POPC) and 0.5 ml of a NaCl 0.3 M solution in Tris buffer. The denser liposomes were isolated by consecutive cycles (at least 3) of sedimentation (centrifugation at 10,000 rpm for 3 min) and resuspension of the sediment with 0.5 ml of 0.3 M NaCl solution in Tris buffer after each sedimentation cycle. Liposome suspensions (60 µL) were incubated with PS solutions (1 mL) in Tris buffer. After 60 minutes of incubation, an additional centrifugation step was used to separate the aqueous and lipid fractions[41]. The lipid fraction was dissolved in 2 mL of a 90 mM SDS solution containing 10% Triton X-100, to solubilize

the lipids and at the same time avoid the formation of PS aggregates. The absorption spectrum of the solution resulting from the lipid fraction was recorded, with Abs_L being its maximum absorbance using a Shimadzu UV-1800 spectrophotometer. By adding the same surfactant solution to the PS solutions, the absorbance of 100% of the free complexes (Abs0, corrected by dilution) was measured. The partition of the PS between the membrane (m) and the aqueous solution (s) was defined by the logarithm of the distribution ratio ($P_{m/s}$), therefore:

Equation 1 $$\log P_{m/s} = \log[Abs_L/(Abs_0 - Abs_L)]$$

This value can be compared to the logarithm of the octanol / water partition coefficient ($\log P_{o/w}$).

2.2.5 Membrane Permeabilization (Attachment 2)

Carboxyfluorescein Leakage

A liposome suspension was prepared using 7.5 mg of lipids and 250 µL of a 50 mM solution of carboxyfluorescein (CF) in a Tris buffer for hydration. The liposomes were homogenized by an extruder with polycarbonate membranes (50 nm). Then, the non-encapsulated CF was removed by size exclusion chromatography, using a chromatographic column (Sephadex G-50) in equilibrium with a 0.3 M NaCl Tris buffer[52] The fraction containing liposomes can be identified visually (yellowish brown portion) and collected in a bottle. As the concentration of CF inside the liposomes is high enough

to promote aggregation, the CF self-suppresses, so an increase in CF fluorescence indicates a leak, that is, a damage to the membrane.[52] Liposome suspensions were always used on the same day they were prepared. The quantification of membrane damage was performed in a flowering microplate with 96 wells with a transparent bottom (300 µL). The wells had a constant volume of lipids (10 µL) and the PS concentration was varied. Each well was filled to 200 µL with a 0.3 M NaCl solution in Tris buffer. It was also used a control containing only lipids and buffer (called blank) and another control containing lipids, buffer and triton (called Triton), that is, a control with free CF. The microplate was irradiated ((from 1.7 to 2.1 mW cm^{-2}) and the fluorescence monitored as a function of the irradiation time with a SpectraMax i3 microplate reader (Endpoint, excitation at 480nm [bandwidth 9nm], emission at 517 nm [bandwidth 15nm], with linear shaking 5 s pre-reading, 50 flashes, background reading). At the end of the experiment, Triton X-100 was added to each well, and the fluorescence intensity was recorded (I_T). For each value of I, the percentage of CF release can be calculated:

Equation 2 $$\%CF_{leaked} = 100\%(I - I_0)/(I_T - I_0)$$

Where, I_0 is the initial fluorescence intensity.

$\%CF_{leaked}$ can be plotted as a function of time (t), and when substantial membrane damage is observed, the curves can be adjusted for a Boltzmann sigmoidal function:

Equation 3 $$\%CF_{leaked} = A_2 + (A_1 - A_2)/[1 + e^{(t-t50)/dt}]$$

Wherein A_1 is the initial $\%CF_{leaked}$, A_2 is the final $\%CF_{leaked}$, t_{50} is the time where the value of $\%CF_{leaked}$ is around 50% and d_t is a parameter related to the duration of the period where the $\%CF_{leaked}$ rapidly changes.

Giant Unilamellar Vesicles

Unilamellar giant lipid vesicles (GUVs) were prepared by using an electroforming method.[53] In short, 10 mL of a 2 mM solution of chloroform lipids were spread on the surfaces of two conductive glasses (coated with tin fluoride oxide), which were placed with their conductive sides facing each other separated by a thick Teflon frame. This chamber was filled with 0.2 M sucrose solution and connected to an alternating generator at 2 V and 10 Hz frequency for 2 hours at room temperature. The vesicle solution was transported into an Eppendorf vial and kept at 4 °C prior to use. To create asymmetry between the inside and outside of the vesicles, 50 mL of the GUV solution was mixed with 300 mL of a 0.2 M glucose solution. The osmolarities of glucose and sucrose solutions can be measured with a cryoscopic osmometer and matched to avoid osmotic pressures. The difference in density between the internal and external solutions forces the vesicles to accumulate at the bottom, where they can be observed. In addition,

the difference between the refractive index of sucrose and glucose solutions provides a better contrast when observed by phase-contrast microscopy. For vesicle membrane damage experiments, different concentrations of PS were dissolved in a glucose solution.

The vesicles were observed with an inverted microscope. Images were recorded with a digital camera. The lighting system was kept in low light intensity to observe the vesicles. Irradiation of samples was performed with an Hg lamp using a filter suitable for photoactivation of the PS (F05 – 395 nm to 440 nm).

Visualization of the effect induced by PS photoirradiation on GUV will be accompanied by optical contrast fading and quantified by taking into account the changes in the brightness intensity using the Image J sofware (National Institutes of Health, Bethesda).[54]

Cell culture

The cell types used were neuronal cells (HT22). The DMEM medium was used supplemented with 10% (v/v) fetal bovine serum (SFB) (GIBCO/BRL Life Technologies) and penicillin-streptomycin solution with 1% (v/v) antimycotic. All cells were provided by Amalia Olga´s lab and were cultured under an atmosphere of 5% CO_2 at 37 °C. The photosensitizer solution was incubated with the cells for 22 to 24 hours, the medium was removed and replaced by PBS during the irradiation, the irradiance used was of 10 J

cm^{-2}. After irradiation, the PBS was removed, and a new medium was added to the wells. The cell viability was analysed after 24 hours of the irradiation.

2.2.6 Data Analysis

Data analyses were performed in Microsoft Excel, Prism and in Origin. Images were analysed by the ImageJ software. The results were presented in the form of means with standard deviations.

2.3 Results and Discussion

2.3.1 Photophysical Parameters

Photophysical parameters of the photosensitizers (PS), such as absorption coefficients (ε_λ), fluorescence quantum yield (Φ_f) and singlet oxygen generation quantum yield (Φ_Δ) were characterized. Absorption spectra were measured according to the method described above. For the chloride salt complexes, the absorption spectra were obtained in water (figure 5), and for hexafluorophosphate salts the absorption spectra were obtained in acetonitrile (ACN) (Figure 6).

In general lines all the complexes have strong absorbance in the blue spectral region (between 400 and 500 nm). It is possible to observe that the spectra of $[Ru(bpy)_3]Cl_2$ has similar bands both in water and in ACN, demonstrating no tendency for aggregation. However, note also that $[Ru(bpy)_3]Cl_2$ has better band definition

compared with the spectra of $[Ru(tpy)(5CNU)_3]Cl_2$ and $[Ru(tpy)(ACN)_3]Cl_2$, suggesting that these latter two ruthenium complexes do tend to aggregate. The emission spectra and the effect of salt (below) will confirm this interpretation. The molar absorptivity coefficients (ε_λ) were calculated for the absorbance peaks found in that region (table 2). In the cases of aggregating complexes, the values calculated and showed in table 2 are not formally ε_λ, but instead the absorption efficiency.

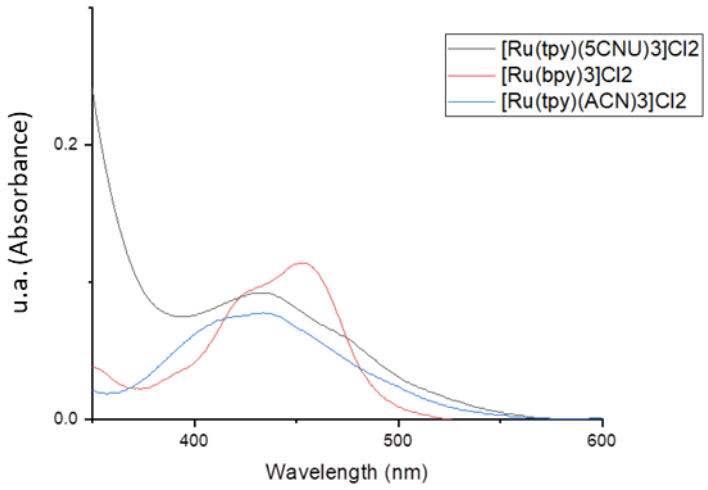

Figure 5. Absorption spectrum of the ruthenium complexes in water. $[Ru(tpy)(5CNU)_3]Cl_2$ 0,02mM, $[Ru(tpy)(ACN)_3]Cl_2$ 0,02mM, $[Ru(bpy)_3]Cl_2$ 0,008 mM.

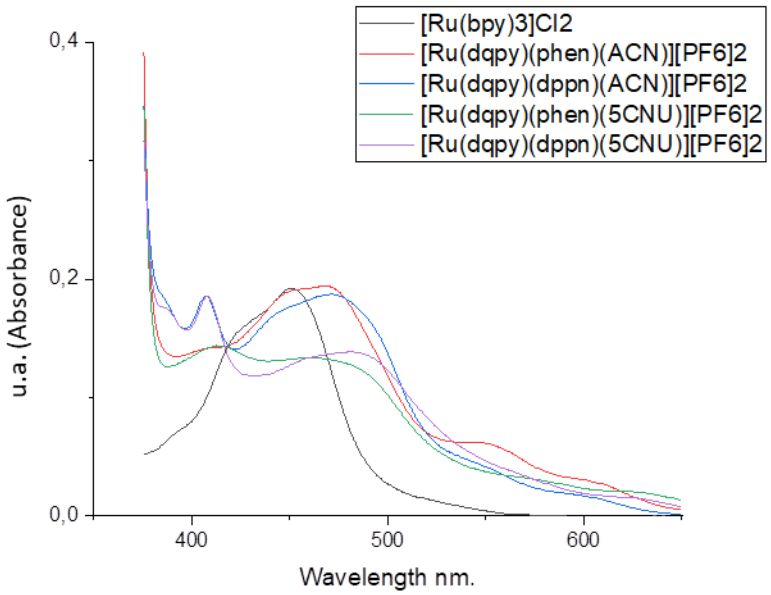

Figure 6. Absorption spectrum of the ruthenium complexes in ACN.

Table 2. Molar absorptivity, quantum yields fluorescence and singlet oxygen generation.

Photosensitizer	Molar Absorptivity Coefficient (ε_λ)[a,b,d]	Fluorescence Efficiency (n_f)[a,c,d]	Singlet Oxygen Quantum Yield (Φ_Δ)[a,c,d]	Singlet Oxygen lifetimes (ns)
$[Ru(bpy)_3]Cl_2$	14600 $M^{-1}cm^{-1}$ / 452 nm[a]	0,040[a] ; 0,018[c]	0,57[c]	66[c]
$[Ru(tpy)(ACN)_3]Cl_2$	4000 $M^{-1}cm^{-1}$ / 434 nm[a]	0,00016[a]	0,02[c]	57[c]
$[Ru(tpy)(5CNU)_3]Cl_2$	4500 $M^{-1}cm^{-1}$ / 420 nm[a]	0,00016[a]	0,03[c]	63[c]
$[Ru(dqpy)(phen)(5CNU)][PF_6]_2$	6932 $M^{-1}cm^{-1}$ / 408 nm[b]	0,0014[c]	0,03[c]	62[c]
$[Ru(dqpy)(phen)(ACN)][PF_6]_2$	6728 $M^{-1}cm^{-1}$ /	0,0035[c]	0,16[c]	65[c]

	464 nm[b]			
[Ru(dqpy)(dppn)(5CNU)][PF_6]$_2$	11661 $M^{-1}cm^{-1}$ / 469 nm[b]	0,0067[c]	0,41[c]	65[c]
[Ru(dqpy)(dppn)(ACN)][PF_6]$_2$	9771 $M^{-1}cm^{-1}$ / 467 nm[b]	0,00013[c]	0,31[c]	65[c]
1,9-Dimethyl-Methylene Blue	78000 $M^{-1}cm^{-1}$ 651 nm[d]	0,05[d]	0,71[d]	

[a]at H_2O, [b]at 5% DMSO in 95% H_2O, [c] in ACN, [d] in ethanol

As for the case of absorption spectra, the emission spectra were also obtained in water for complexes with chloride counterion (figure 7, excitation at 431 nm), and in ACN for complexes with hexafluorophosphate counterion (figure 8, excitation at 416 nm). Note that the compounds that showed broader absorption bands in water are those that also showed almost no fluorescence, indicating the presence of aggregation. Some of the hexafluorophosphate Ruthenium complexes dissolved in ACN also showed small fluorescence emission. Although these complexes have faster or slower rates of intersystem crossing, which may cause lower or stronger fluorescence emission, the absence of fluorescence emission does suggest that they may also aggregate. Quantification of fluorescence efficiency was performed were calculated using a $[Ru(bpy)_3]Cl_2$ solution as a standard and values are showed in Table 2.

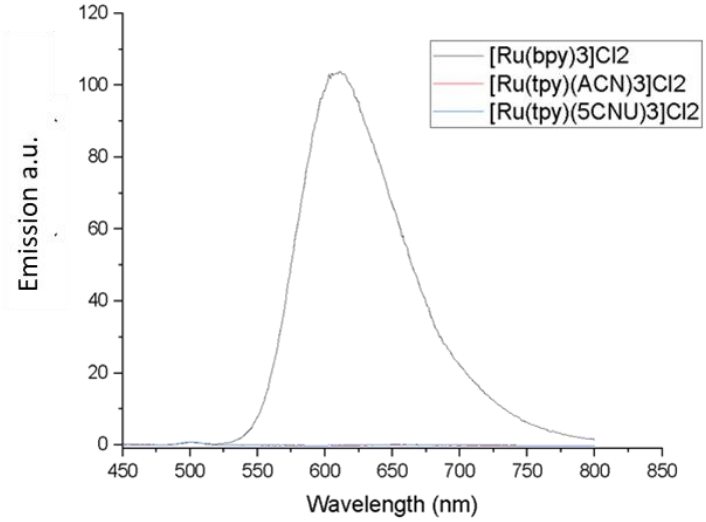

Figure 7. Emission spectrum of the Ruthenium complexes in water. $[Ru(tpy)(5CNU)_3]Cl_2$ 0,02mM, $[Ru(tpy)(ACN)_3]Cl_2$ 0,02mM, $[Ru(bpy)_3]Cl_2$ 0,008 mM.

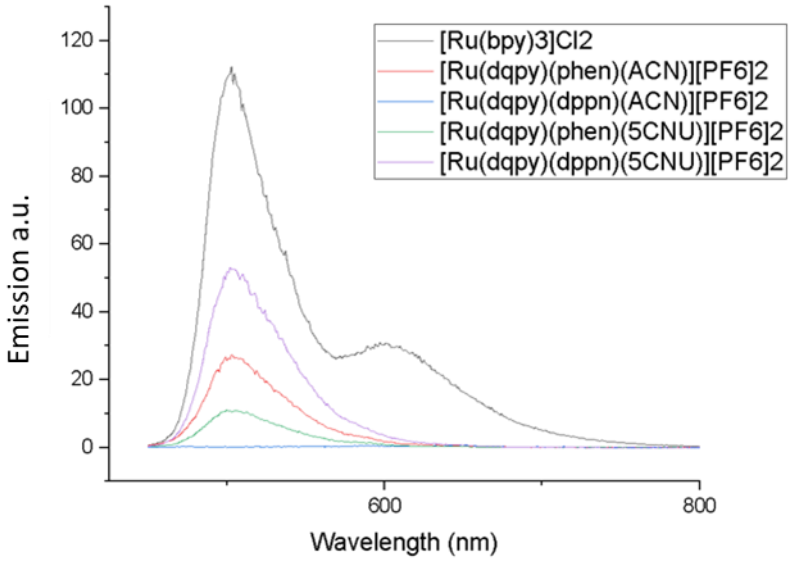

Figure 8. Emission spectrum of the Ruthenium complexes in ACN.

In order to evaluate the generation of triplets and its deactivation to form singlet oxygen, we measured light emission at 1270 nm (figure 9), which is the characteristic spectral region in which singlet oxygen has its phosphorescence emissive decay $^1O_2$ ($^1\Delta_g$) to ground state molecular oxygen. By comparing the emission intensity at 1270nm with the phosphorescence emission at 1270 nm of Methylene blue (Φ_Δ =0.5), we were able to estimate the quantum yields of singlet oxygen generation (Φ_Δ) for the ruthenium complexes. By analysing the kinetic emission decay at 1270nm we were also able to quantify the singlet oxygen lifetimes (table 2).

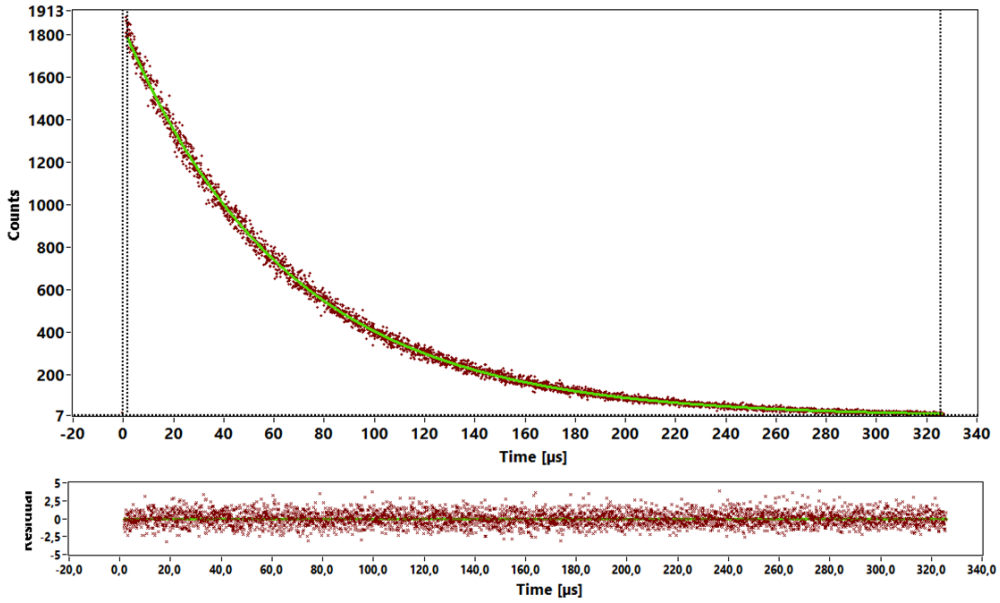

Figure 9. Phosphorescence emitted by singlet oxygen decay in ACN. The PS was $[Ru(bpy)_3]Cl_2$.

It is noted that all tested complexes have low fluorescence efficiencies (less than 0.040). Note also that only the complexes with the DPPN ligand have significant singlet oxygen generation yield (greater than 0.3), while other complexes showed very low level of singlet oxygen generation (less than 0.2).

As can see in Table 2, some of the studied complexes generate almost no singlet oxygen, The formation of singlet oxygen is always related to the formation of triplets that are stable and that live long enough to react with oxygen. In many of these complexes the rate of intersystem crossing is so fast that it ends up generating triplets but that do not live long enough to react with oxygen, i.e., they quickly decay to ground state). In the case of complexes that form singlet oxygen there is an efficient internal energy transfer (metal-ligand) in such a way that the triplet state of the ligand is efficiently populated, which efficiently reacts with oxygen, forming singlet oxygen.[47]

2.3.2 Membrane Association

In order to calculate the membrane/solvent partition coefficient ($P_{m/s}$), the ruthenium complexes were incubated in the presence of POPC liposomes, as described in section 3.4. Briefly, the complexes were incubated in the presence of the liposomes, and then the liposomes were separated by centrifugation. The absorption spectrum of the centrifuged solutions was compared with that of the free complex solutions.

Table 3. POPC/H_2O partition ($P_{m/s}$)

Complex	log$P_{m/s}$	Complex	log$P_{m/s}$
$[Ru(bpy)_3]Cl_2$ (452 nm)	-1,15	$[Ru(dqpy)(dppn)(5CNU)][PF_6]_2$ (469 nm)	-0,67
$[Ru(tpy)(ACN)_3]Cl_2$ (434 nm)	-1,80	$[Ru(dqpy)(phen)(5CNU)][PF_6]_2$ (408 nm)	-0,36
$[Ru(tpy)(5CNU)_3]Cl_2$ (420 nm)	-1,52	$[Ru(dqpy)(dppn)(ACN)][PF_6]_2$ (467 nm)	-0,75
		$[Ru(dqpy)(phen)(ACN)][PF_6]_2$ (464 nm)	-0,86

As can be seen, the $[Ru(bpy)_3]Cl_2$, $[Ru(tpy)(5CNU)_3]Cl_2$ and $[Ru(tpy)(ACN)_3]Cl_2$ complexes have largely negative values of log$P_{m/s}$ (log$P_{m/s}$ <-1) indicating that are not efficiently associated with membranes. Note, however, that the other complexes have a slightly higher membrane / solvent partition coefficient, but still having a negative log$P_{m/s}$.

An important factor in the membrane damage mechanism is the association of the complexes with the membrane. In this case, the greater the association of the complexes with the membrane, that is, the greater log$P_{m/s}$ is, the greater the probability of the complex's direct interaction with the phospholipids, facilitating the contact-dependent reactions. As previously mentioned, type I photosensitization generates peroxyl-lipids and truncated lipids with the organic function of carbonyl (aldehydes and ketones), which are the main responsible for impairing the integrity of the membrane.[26]

Furthermore, the diffusion of the singlet oxygen molecule is small in the complex environment of a cell, that is, even for type 2 photosensitization it is important that the complex has a reasonable association with the membrane, in order to increase the probability of the singlet oxygen reaction with phospholipids.

Based on the lower level of membrane interaction based a indicated in the partition measurements, which is a consequence of the high polar character, the interaction of these compounds with biological substrates will depend on other types of forces, liked electrostatic forces. It is expected that using negative charged lipids in the membranes, such as POPG, one can increase the binding of the positively-charged complexes to the membranes. Obviously, one could always increase $logP_{m/s}$ by complexing ruthenium with ligands having greater lipophilicity,.

2.3.3 Membrane Permeabilization

Giant Unilamellar Vesicles Experiment

GUVs were prepared by the electroforming method (for more information, see item 2.2.6), using DOPC as the lipid. The ruthenium complexes used for this test were chloride complexes $[Ru(bpy)_3]Cl_2$, $[Ru(tpy)(ACN)_3]Cl_2$ and $[Ru(tpy)(5CNU)_3]Cl_2$, and the hexafluorophosphate complexes $[Ru(dqpy)(phen)(5CNU)][PF_6]_2$, $[Ru(dqpy)(phen)(ACN)][PF_6]_2$, $[Ru(dqpy)(dppn)(5CNU)][PF_6]_2$ and $[Ru(dqpy)(dppn)(ACN)][PF_6]_2$.

The hexafluorophosphate complexes were not readily soluble in water, thus they

were prepared by added directly to the lipid film, during the electroforming method. Therefore, for those complexes there was not an irradiated control. The images of the GUVs were recorded from 0 minutes to 60 minutes, as can be seen in figures 10A. Note that there is loss of contrast of the membrane with irradiation, indicating that there was exchange of the glucose that was in the exterior with sucrose that was in the interior (the difference between the refractive index of the internal and external solutions give rise to the membrane contrast). There was also decrease in the size of the membrane, with indicates loss of lipids during the irradiation.[55] The images were analysed by the ImageJ software to determine the size of the GUVs and the loss of contrast in the inside of the GUVs (see method section). The time to lose 70% of contrast for each PS was plotted in the figure 10B, and compared to each PS singlet oxygen generation quantum yield (Φ_{Δ}). The 70% percentage was chosen because it was a number high enough to correlate with loss of membrane integrity, and it was still possible to measure robust data.

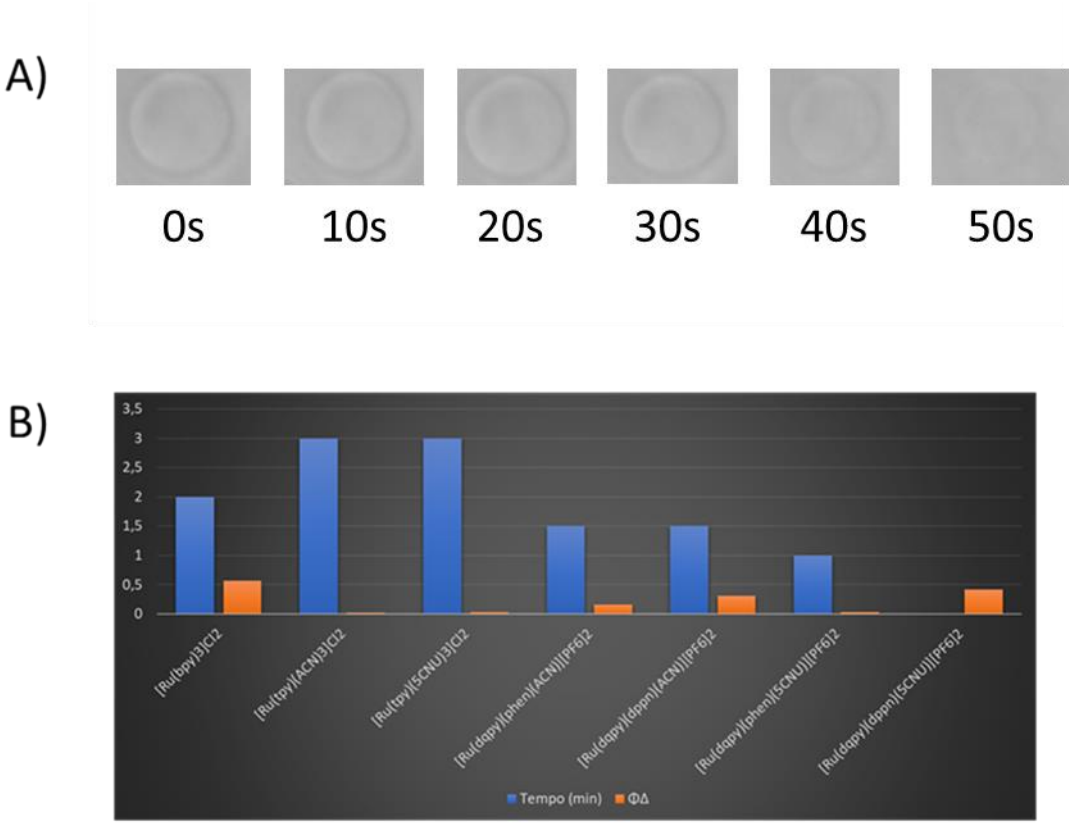

Figure 10. Image of GUV being observed as a function of time (in minutes). B. Time to lose 70% of contrast (blue bars) and singlet oxygen quantum yield (orange bars).

As can be seen on figure 10B, except the complex $[Ru(dqpy)(dppn)(5CNU)][PF_6]_2$, all other complexes were able to damage and to permeabilize the membranes, providing loss of contrast, which is shown as blue bars in Figure 10B. The complex $[Ru(dqpy)(dppn)(5CNU)][PF_6]_2$ only caused an increase of fluctuation of the membranes. It is also noted that the time necessary to lose contrast is not proportional to the singlet oxygen generation quantum yield production. However,

compounds that have less negative logPm/s, which are the complexes that have the (dqpy)(phen) and the (dqpy)(dppn) ligands (Table 3) show higher efficiency of membrane leakage. As mentioned before, the formation of membrane pores are correlated with the formation of lipid truncated aldehydes, which are dependent on the contact-dependent reaction and not so much on the yield of singlet oxygen generation.[26]

In resume, when PS reacts with membranes by the contact independent pathway the double bonds present are promptly oxidized to hydroperoxides, which can increase the fluidity of the membrane, facilitating the permeabilization, but not the loss of membrane integrity. However, when PS reacts with membranes by the contact dependent pathway the lipids are oxidized to ketones, aldehydes and others oxidations states, which can lead to loss of membrane integrity.

Thus, this further agrees with the current knowledge, which indicates that the singlet oxygen generation is not the main factor in membrane permeabilization. In fact, when the membrane partition coefficient found previously is accounted, it is possible to see that the complexes with higher lipophilicity are the ones that cause more damage in less time, indicating a contact dependent pathway.

2.3.4 Cell phototoxicity studies of $[Ru(bpy)_3]Cl_2$

Although it will be interesting to correlate the cell cytotoxic of ruthenium

complexes with their respective molecular structure, we only delivered in this dissertation the material of initial studies of $[Ru(bpy)_3]Cl_2$ in HT22 cell culture. Control experiments were performed (irradiating cells in the absence of PS and in the presence of medium) and are shown in the next section (Figure 11).

$[Ru(bpy)_3]Cl_2$ is a standard ruthenium complex used in many different fields, such as photophysics, photochemistry and conversion of energy.[56] Thus, it has known properties and behaviour, being a suitable complex to initiate the studies of ruthenium complexes in neuronal cells.[57] The absorption spectrum of $[Ru(bpy)_3]Cl_2$ has an intense band with a maximum of ~450 nm, and it exhibits a high quantum yield of singlet oxygen formation (Φ~0.57 in ACN).

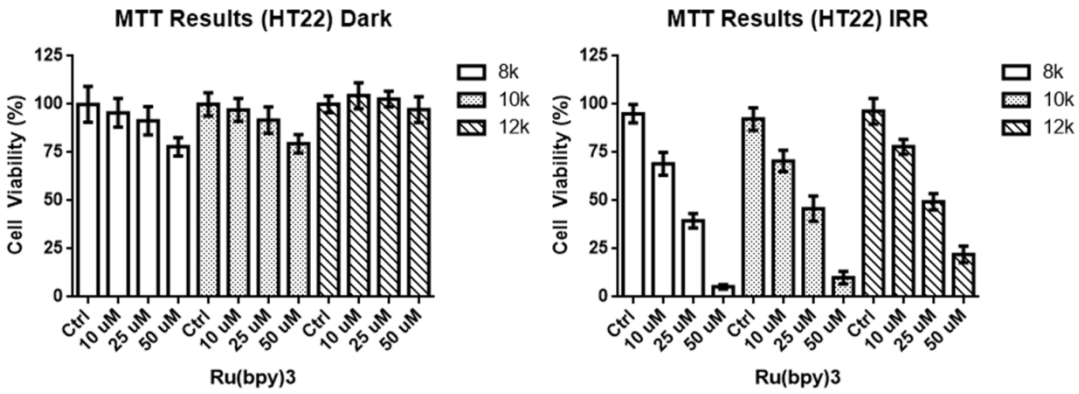

Figure 11. Cell viability by MTT assay, in cells in the dark (Dark) and irradiated with red light (IRR). Percentage is relative to the control in the dark.

Note that the dark cytotoxicity is absent in all conditions tested (Figure 11). Under

irradiation, cell viability decreases proportionally to the concentration of $[Ru(bpy)_3]Cl_2$ in all tested conditions. It is also possible to observe that cells incubated with 25 µM of $[Ru(bpy)_3]Cl_2$ experience significant loss in cell viability when irradiated (IRR), whilst maintaining no cytotoxicity in the dark. Those results seem to be on par with the results obtained by previous groups, wherein the phototoxicity of ruthenium complexes in Hela cells vary in the micro molar concentration range (0.5 µm to 20 µm).[58]

Note also that the lower the amount of cells (from 12000 to 8000 cells) the higher is the efficiency of the $[Ru(bpy)_3]Cl_2$ in terms of causing cell death, indicating that the amount of PS/cell is an important parameter to define the phototoxicity, which may also be explained by a stacking of cells, hampering the uptake of Ps by the cells. The LD50 increases from 17 to 20 and 25 µM for incubations with 8000, 10000 and 12000 cells, respectively. Assuming that the percentage of cell uptake is similar to that quantified previously by Puckett and Barton (~4%,),[59] the intracellular concentrations of $[Ru(bpy)_3]Cl_2$ varies from 0.4 to 2 µM (total concentrations from 10 to 50 µM, respectively) and concentrations per cell varying from 30 pM to 250pM. The LD50 in terms of intracellular concentration per cells kept relatively constant and around 80pM per cell. It will be interesting to compare this number with another obtained with an organic based photosensitizer (DMMB, see below).

To evaluate if the photodamage could be somehow avoided by the use of antioxidant agents, we tested the level of cell viability in the presence of PD (15-

Lipoxygenase (LOX) inhibitor), ferrostatin (ferroptosis inhibitor), CyPPA (positive modulator of small conductance calcium-potassium activated channels), and NAC (antioxidant). Note that none of the used compounds were able to effectively protect cells against the photodamage (Figure 12). This is evidence that the photoinduced reactions are probably caused in specific cellular niches in which the antioxidants are not present. The fact that membrane damage in a local effect caused by the contact-dependent reaction, i.e., reactions occurring in the molecular contact limit of the PS, explain the difficult in finding a proper protecting agent.[26]

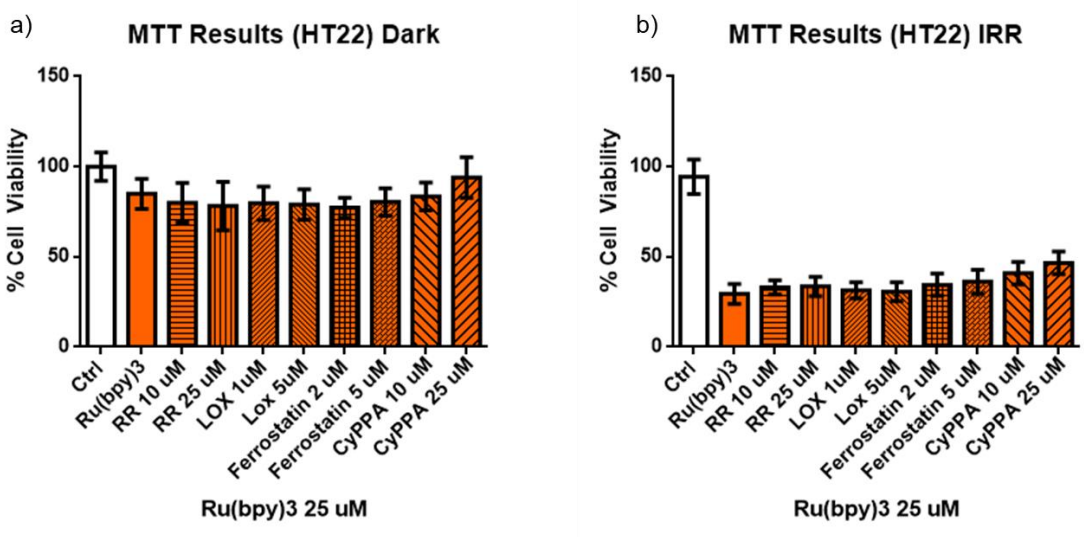

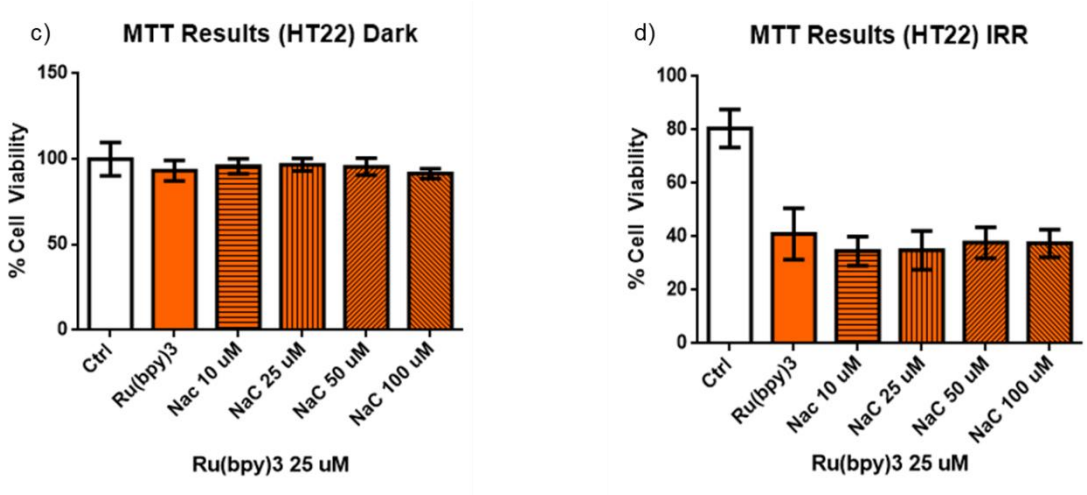

Figure 12. In the graphs we can observe the absorbance of the formazan crystals normalized by the control in the dark. In the graphs a) and b) 10 thousand cells were plated, with 24 hours of incubation time and 10 $J.cm^{-2}$ of irradiance. In the graphs c) and d) 50 thousand cells were plated, with 24 hours of incubation time and 10 $J.cm^{-2}$ of irradiance.

2.4 Conclusions

Although they do not bind efficiently to membranes, ruthenium complexes are able to cause damage in membrane models, and are promising candidates for photochemical therapy, especially PDT. Several authors use as the main parameter to indicate photosensitizer efficiency the singlet oxygen generation quantum yield. In this study, we could observe that the complexes with higher values of membrane partition were the ones with more damage efficiency in GUVs. Wherein the singlet oxygen generation could not be correlated with any of the results obtained. Our data are in consonance with others that indicate that the efficiency of singlet oxygen generation, are not the best parameters to correlate with membrane damage or cell death.[40] Other

factors such as the capacity to induce both type I and type I photosensitization mechanisms, as well as, the intracellular localization of the PS.[45]

The ruthenium complexes have a high yield of formation of triplet excited states and some have a high generation of singlet oxygen, which makes them interesting candidates in the application in PDT[60–62]. Oxidation of lipids by contact dependent and independent pathways has very specific products. We envisage that, the next steps to understand the mechanisms of damage by the ruthenium complexes should comprise the study of the oxidized lipids obtained in the photosensitization protocols.

Chapter 3 – Cell and Mitochondrial damage by photosensitization with DMMB

3.1 Introduction

In the previous studies it was found an indication that ruthenium complexes can cause photochemical damage in membranes models[63], mainly by the contact-dependent pathway (see chapter 2). In this chapter, we investigate the photodamage by a phenothiazinium derivative (DMMB) in cell lines, as to understand with further details membrane and cellular damages, inducing specific mechanisms of cellular damage. DMMB was chosen, since the group had already studied its mechanisms in different situations. [26, 27, 43]

3.2 Materials and Methods

3.2.1 Materials and Cell Culture conditions

The photosensitizer 1,9-dimethyl methylene blue (DMMB) is a phenothiazine dye derived from methylene blue (Figure 13). The absorption spectrum of DMMB has an intense band with a maximum of ~650 nm, and it exhibits a high quantum yield of singlet oxygen formation (Φ~0.7 in ethanol).

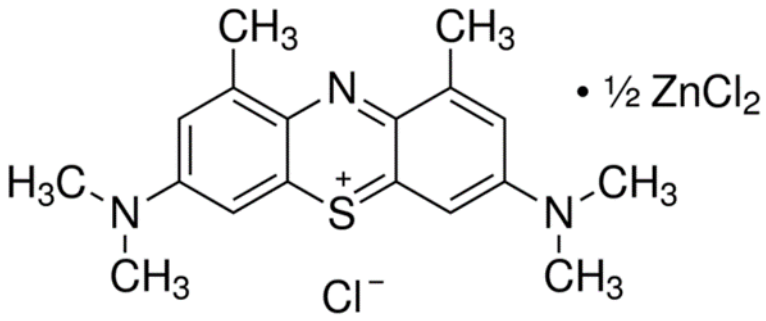

Figure 13. Molecular structure of 1,9-dimethyl methylene blue (DMMB).

The cell line used was a Mouse Hippocampal Neuronal Cell Line (HT22). The cells were cultivated in Dulbecco's Modified Eagle Medium (DMEM) supplemented with 10% (v/v) fetal bovine serum (FBS), 2% (v/v) streptomycin/penicillin and 1% (v/v) of sodium pyruvate in an incubator at 37 °C with 5% CO_2.

3.2.2 Photosensitization Protocol

The cells were seeded in 96 well plates (100 µL) for at least 18 hours prior to the treatment. The cells were then incubated with PS for 6 hours to 24 hours, for this step PS stock solutions in ultrapure water were diluted in medium. After the incubation, the cells were washed with 100 µL of PBS, and 100 µL of clean PBS was added for the irradiation step.

The plates were irradiated, with the lids on, for 20 minutes using LEDs. The light fluence used varied from 10 to 20 J cm^{-2}, measured with a dosimeter. After the irradiation

the PBS was removed and 100 µL of fresh medium was added. For this step, two identical plates were prepared; one was irradiated (IRR) and the other one was left covered in aluminium foil next to the irradiation chamber (Dark).

3.2.3 Cellular viability by MTT assay

Cell viability was analyzed by the metabolic activity using a MTT (3-(4,5-dimethylthiazol-2-yl)-2,5- diphenyltetrazolium bromide) assay. MTT is a compound soluble in aqueous solution, yellow in colour, and is internalized by the cells where it complexes with mitochondrial enzymes being reduced to formazan crystals. The formazan crystals were solubilized with dimethyl sulfoxide (DMSO) and quantified by the absorption measurement at 570 nm. The cell viability was calculated relative to the absorbance of a non-photosensitizing control (considered as 100%).

In summary a MTT solution of 0.5 mg/mL was added to each well after 24 hours of the photosensitization, and then the plates were incubated for 1 hour at 37 °C in an atmosphere with 5% CO_2. Afterwards the MTT solution was removed and the plates were frozen for at least one hour. For reading it was added DMSO to each plate, and the solutions were homogenized in a shaker for 30 min (120 rpm, 37 °C) and the absorbance of the wells were recorded in a plate reader, at 570 nm, using a wavelength without absorption of the formazan crystals as a reference wavelength, in this project the chosen wavelength is 630 nm.

3.2.4 Potential Protective Agents

In an attempt to understand better the interactions of the PS with the Cell, some potential protective agents were used. Those agents are known for targeting specific proteins in the mitochondria. Therefore, if some of those compounds display some protection from cellular death, which would be indicated by a lower scope of action of those protective agents, would be possible to specify the PS mechanism of action, or at least diminish the scope of action of those PS.

Ruthenium Red (RR) is the common name of ammoniated ruthenium oxychloride, a known mitochondrial calcium uptake blocker, by inhibiting mitochondrial calcium uniporter.[64] The inhibition of calcium uptake in cells can be protective since damage on the cells can increases the level of calcium in the cells, which in turn could dysregulate many processes in the mitochondria, leading to cell death.

Ferrostatin-1 (Fer-1) is an inhibitor of ferroptosis, is a non-apoptotic form of cell death, caused by the accumulation of iron, which can catalyse lipid peroxidation. The ferrostatin-1 acts by inhibiting lipoxygenases and as radical trapper, thus preventing the cell death.[65]

PD (126176) is a 15-Lipoxygenase (LOX) inhibitor, an enzyme responsible for production of inflammatory leukotrienes. During glutamate-induced oxidative stress, mitochondria of neuronal cells can be damaged by 15-lipoxygenase by a unknown

mechanism, decreasing the mitochondria membrane potential and leading to cell death.[66]

CyPPA is a positive modulator of small conductance calcium-potassium activated channels (SK Channels), these channels protect the neuronal cells in different paradigms of cell death triggered by H_2O_2, glutamate, or endoplasmic reticulum stress.

N-acetylcysteine (NAC) is a precursor of glutathione (GSH), and it is a capable scavenger of cell ROS.[67] As mentioned, cell ROS can activate a cascade of reactions leading to different types of cell death. In addition, NAC being a precursor of GSH, it also triggers production of GSH, which is an important regulator of ROS in cells.[68,69]

3.2.5 Flow Cytometry Assays

After 24 hours of the Irradiation Protocol, 0.5 µL of the fluorescent probes solution was added to each well, and the plate was incubated for several minutes at 37 °C, 5% CO_2. Then the medium of each well was collected to a specific tube, and the wells were washed with PBS, the PBS was collected in the same tubes and was added trypsin to each well, and the plates were incubated for 2 to 3 minutes. Fresh medium was added to each well and the resulting solution was collected in each tube. The tubes were then centrifuged for 5 minutes at R.T., 2000 rpm. The supernatant was removed and the pellet formed was resuspended in PBS. The final solution was transferred to FACS tubes for reading.

MitoSOX

A stock solution of 1.25 mM of MitoSOX™ Red in DMSO was prepared in advance and stored in a -20°C freezer. The plate was incubated with staining solution for 30 minutes.

Bodipy

A stock solution of 2 mM of BODIPY® 581⁄591 C11 in DMSO was prepared in advance and stored in a -20 °C freezer. The plate was incubated with staining solution for 60 minutes.

3.2.6 MitoTracker

The photosensitization protocol was made as described above, in a 24 well plate (500 µL per well, 30 thousand cells per well), and each well contained a coverslip.

After the photosensitization protocol, the medium was removed and the cells were incubated for 30 min at 37 °C with a new medium without serum and with 200 nM MitoTracker (500 µL per well).Since MitoTracker is sensible to light, the light was off when handling and incubating the cells. After the incubation, the medium was removed and the cells were fixed. The protocol of fixation of the cells was as follow: the medium was removed, PBS 1x (500 µL per well) was added for 5 min at 37 °C; PBS was removed, 500 µL per well of paraformaldehyde (PFA 4%) was added for 25 min at room temperature (RT); PFA was removed, PBS 1x (500 µL per well) was removed.

Following the fixation of the cells the coverslips were mounted in a microscope slide for microscope imaging. Briefly, the coverslips were removed from the well and treated with DAPI and mounted in the rectangular slide with the face containing the cells on contact with the microscope slide. After the slide was dry, the coverslips were fixed with nail polish. All the protocols were made without using light. The microscope used for imaging was Leica DM 4000B.

3.2.7 Data Analysis

Data analyses were performed in Microsoft Excel, Prism and in Origin. Graphics and curve fittings were plotted in Prism and FlowJo. The results were presented in the form of means with standard deviations.

3.3 Results and Discussion

3.3.1 MTT Assay

Effect of Light and Photosensitizers (PS)

Initially, the cells were irradiated in the absence of the PS to test if the light alone was causing damage. In addition, the cells were also irradiated in the presence of culture medium to test its influence in the viability of cells. Two different types of LEDs were tested, one emitting red light, 660 nm ±10nm, and the other emitting blue light, 465 nm ±10nm (Figure 14).

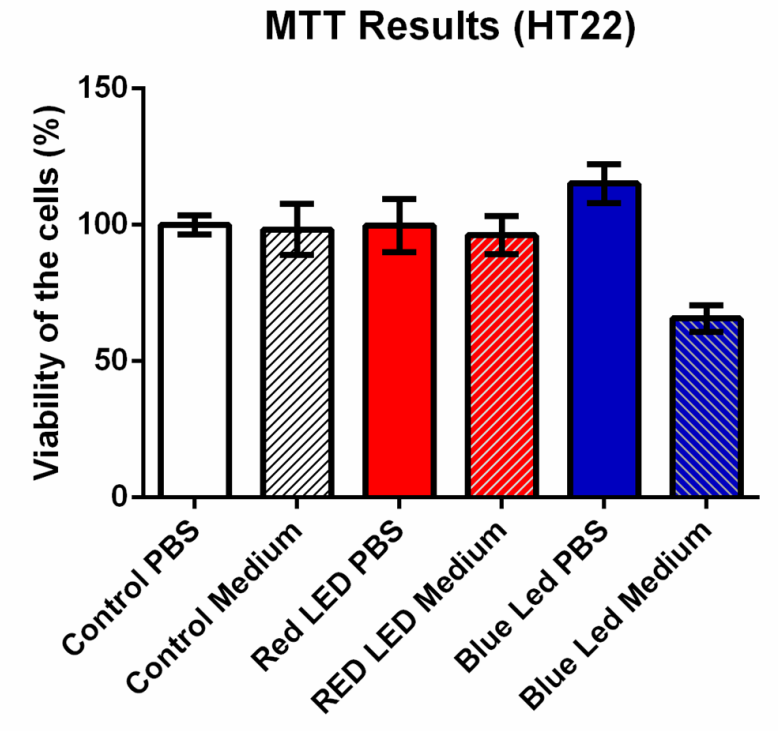

Figure 14. Cell viability by MTT assay, percentage is relative to the control with PBS. Red-light LED (660 nm ±10nm), and blue-light LED (465 nm ±10nm).

As observed in figure 14, cell viability as measured by MTT is constant and close to 100% to all conditions tested with the exception of irradiation with blue light in the presence of medium, which has a decrease to 60%, therefore we can see that blue light caused damage in cells containing medium, which was already described in the literature.[55,70] This occurrence is explained by the fact that DMEM medium contain flavins (such as riboflavin) and aminoacids (such as tryptophan) which absorb blue light and generate ROS, acting as PS. As to avoid additional damage caused by the blue light, the cells incorporated with the PSs were irradiated in the presence of fresh PBS.

The photosensitizer solution (DMMB) was incubated with the cells for 1 to 6 hours, and the irradiance used was of 10 to 20 J.cm^{-2}. The cell viability was analysed after 24 hours of the irradiation (Figure 15).

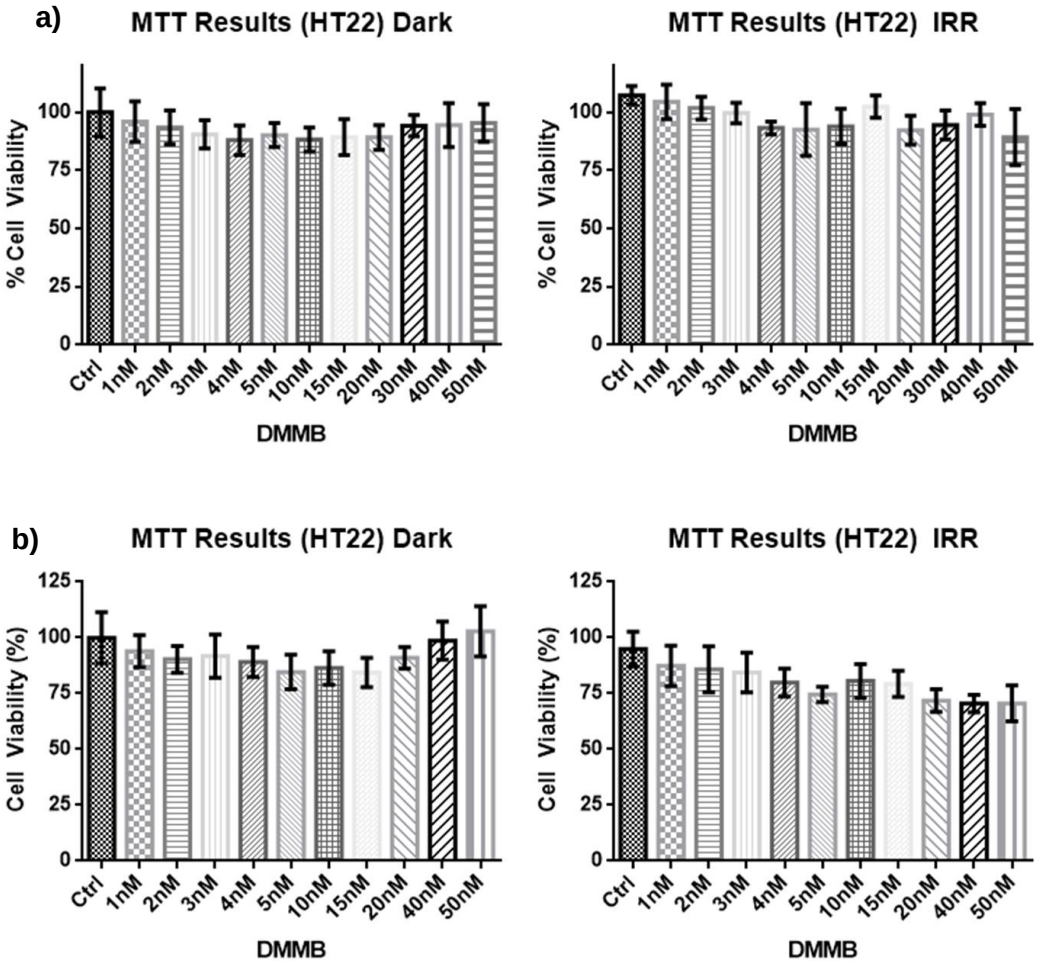

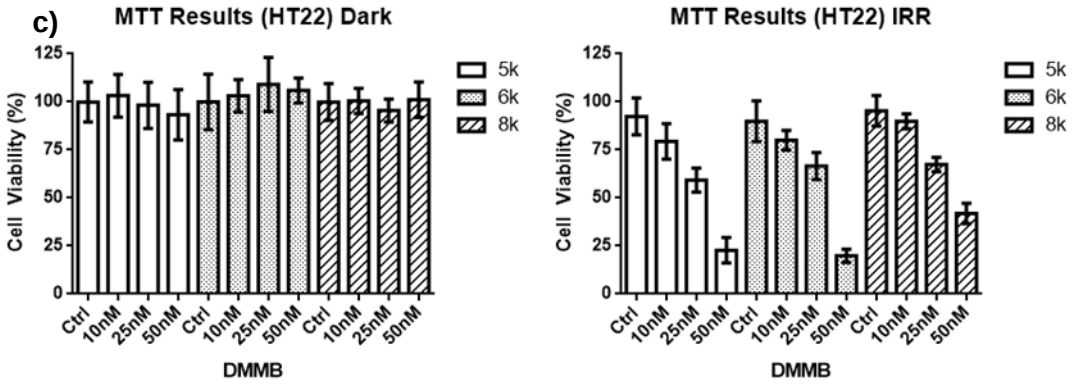

Figure 15. Cell viability by MTT assay, percentage is relative to the control in the dark. In a) the incubation time was 1h, the light dosage was 10 J.cm^{-2} and ten thousand cells were seeded. In b) the incubation time was 3h, the light dosage was 20 J.cm-2 and ten thousand cells were seeded. In c) the incubation time was 6h, the light dosage was 20 J.cm-2 and five thousand, six thousand and eight thousand cells were seeded.

The viability of cells treated with DMMD and red light was tested in different concentrations (1 nm to 50 nM, figure 15a and 15b), however DMMB did not cause significant loss of viability in incubation times lower than 6 hours and with cell density of 10.000 per well. With 6 hours incubation it was not possible to determine loss of viability in the dark, therefore having low cytotoxicity in the absence of irradiation. However, the cells displayed significant loss of viability (around 50% or higher)[71] at concentrations higher than 25 nM when irradiated. Previous studies had found that Methylene Blue (MB), a similar phenothiazinium compound to DMMB, has a protective effect on cells (50% higher cell viability, when compared to control) exposed to hypoxia-reoxygenation stress. These results are intriguing, since the DMMB could also act double as a protective agent in the presence of ROS (during the re-oxygenation stress), and as a PS

causing photochemical damage.

Note also that the lower the number of cells (from 5000 to 8000 cells) the higher is the efficiency of the DMMB in terms of causing cell death, indicating that the amount of PS/cell is an important parameter to define the photocitotoxicity. The LD50 increases from 30 to 35 and 40 nM for incubations with 5000, 6000 and 8000 cells, respectively. Assuming that the percentage of cell uptake is similar to that quantified previously to be ~30%,[72] the intracellular concentrations of DMMB varies from 9, 10 and 12 nM and the intracellular concentrations of DMMB are around 2 pM/ cell, which is a lot smaller than the concentrations of $[Ru(bpy)_3]Cl_2$ per cell at the LD50 (80pM/cell). This difference indicate that even considering the different level of PS incorporation, DMMB is a PS lot more efficient than $[Ru(bpy)_3]Cl_2$ in terms of causing cell death. This is probably because of the specific intracellular locations of DMMB and the consequent induction of regulated cell death mechanisms.[72]

Potential Protective Agents

In an attempt to understand if the photochemical damage caused by the PSs was disrupting some of the cell pathways of the neuronal cells, some common potential protective agents were tested in the presence of the PSs, in an endeavour to prevent loss of cell viability. Those agents were tested in a viability assay, more specifically using MTT. The MTT results using those agents can be seen on figure 16.

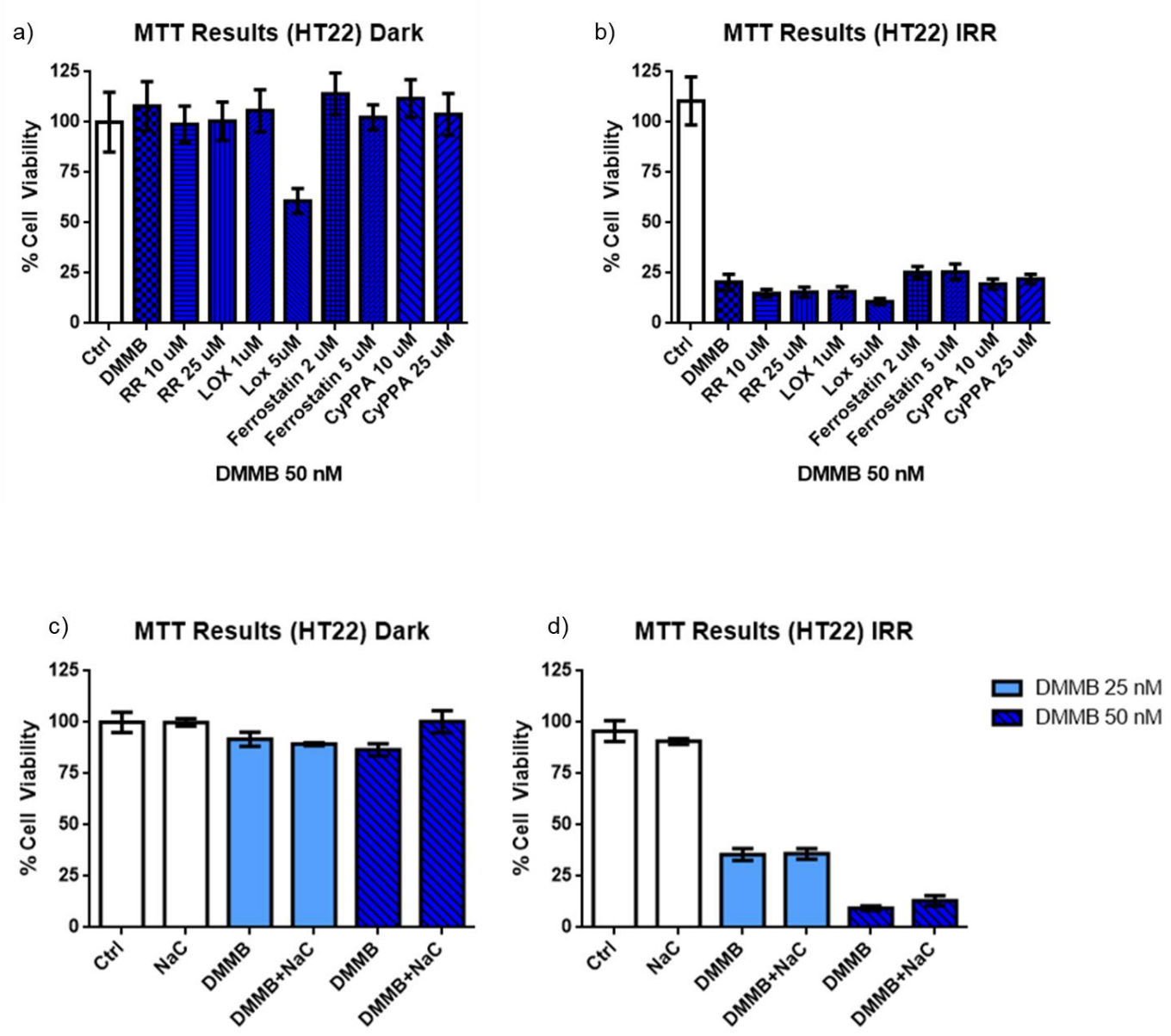

Figure 16. In the graphs we can observe the absorbance of the formazan crystals normalized by the control in the dark. In the graphs a) and b) 6 thousand cells were plated, with 6 hours of incubation time and 20 $J.cm^{-2}$ of irradiance. In the graphs c) and d) 50 thousand cells were plated, with 6 hours of incubation time and 20 $J.cm^{-2}$ of irradiance.

The MTT results displayed that in the dark the percentage of cell viability is close to 100%, and in the presence of irradiation (IRR) the loss of cell viability was similar to the results obtained in the absence of the potential protective agents. The only exception was the results obtained with the LOX inhibitor, that when combined with DMMB, was cytotoxic to the cells (~40% loss of cell viability) even in the dark, indicating that these compounds may react forming a new compound which could be leading to loss of cell viability. The results displayed on the figure 16 indicate that none of those compounds were capable to protect the cells from the damage caused by the PS. Thus, indicating that the PDT is a treatment with low chance of resistance, not being hindered by ROS scavengers, ferroptosis inhibitor (lipoxygenase inhibitor), calcium uptakes blockers and even SK channels modulators.

Probably those compounds could not prevent the photochemical damage, because singlet oxygen and excited PSs react very fast and promptly with nearby molecules (short diffuse time in the cytoplasm). In addition, reactive species are probably generated in a specific environment, oxidizing many different targets in a small time-window. It is likely that the antioxidant used to not concentrated at enough concentration in the sites of photodamage. Thus, as stated before, previous knowledge of intracellular localization of the PSs is more important to try to prevent the photochemical damage instead of using common potential protective agents. In order to better characterize the site-specific photomage, some assays to evaluate structure and function of mitochondria

were performed before and after photodamage.

3.3.2 Markers of mitochondrial damage

MitoSOX is a specific marker of mitochondrial damage. As can be seen on figure 17, the DMMB treatments in the dark causes no increase in the emission of MitoSOX. However, both experiments show an expressive increase in the MitoSox fluorescence in the presence of PS and irradiation. This probes responds to the oxidation environment and the significant increase the probes oxidation is compatible with the generation of reactive oxidants in mitochondria of irradiated cells previously treated with DMMB. The figure 17 shows an increase in percentage of gated population of cells with fluorescence of the MitoSox probe, which is activated in the presence of ROS. Therefore, DMMB generates ROS at the mitochondria upon irradiation.

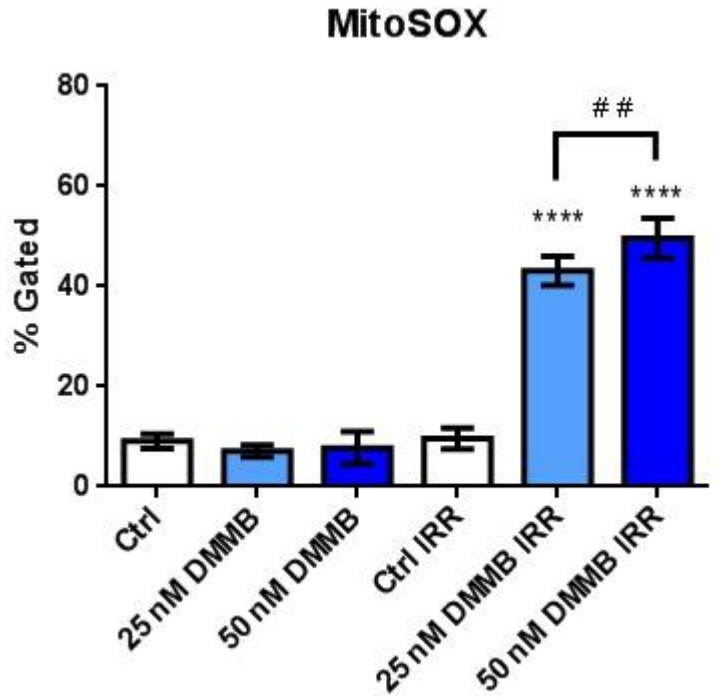

Figure 17. Mitochondrial oxidation of HT22 cells treated with DMMB. Gated MitoSox fluorescence emission of untreated HT22 cells (control), HT22 cells treated with DMMB (25 and 50nM) and kept in the dark and HT22 cells treated with DMMB (25 and 50nM) and irradiated.

It is known that DMMB interacts efficiently with membrane mimics and cause photodamage and leakage.[52] BODIPY® 581/591 is a bodipy dye attached to undecanoic acid, which can be used to detect reactive oxidants in cells and membranes. Oxidation of the polyunsaturated butadienyl portion of the dye results in a shift of the fluorescence emission peak. Interestingly, DMMB treatment displays an increase in peroxidation of lipids, as can be seen by the shift in gated emission of the BODIPY probe (red). The figure 18 shows an increase in the percentage of lipid peroxidation in the gated cells. In

summary, the DMMB is acting both in mitochondria and in the lipids (lysosomes) as already was predicted, since it was shown in previous studies in different cell lines.

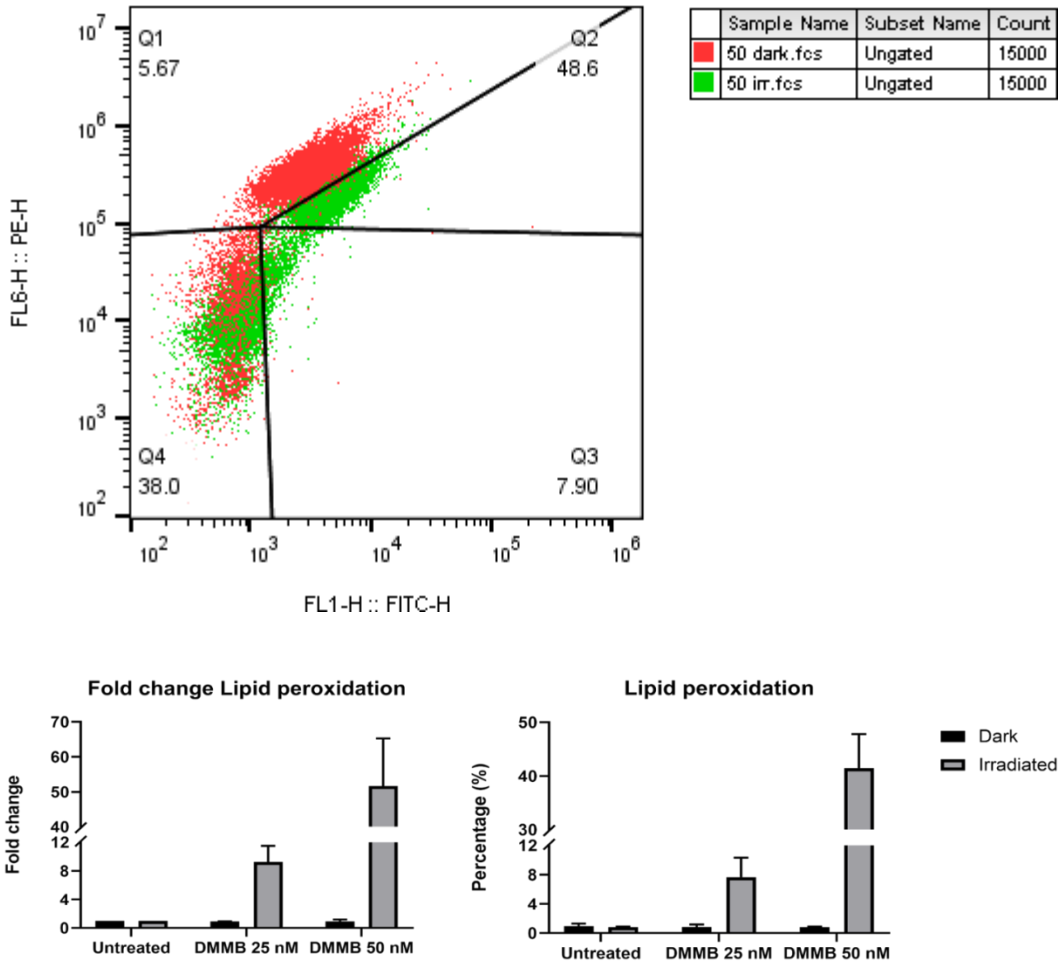

Figure 18. Lipid oxidation in HT22 cells. (Above) FACS data of control (untreated) and treated with DMMB at 25nM and irraditated. (Below) Bodipy emission in fold change of untreated HT22 cells (control) and HT22 cells treated with DMMB at 25 and 50nM and irradiated.

Grohm et al. proposes a method to evaluate and catogorize mitochondrial

morphology by microscopic evaluation of cells stained by mitotracker. In resume, mitochondria are complex and dynamic organelles that undergo many different processes such as fusion and fission, which can permanently cause morphology changes on the mitochondria. In addition, such processes can be disturbed by oxidation process, causing very specific morphology changes.

We evaluated the effect of DMMB and light in mitochondria morphology changes. Mitochondrial morphology changes can be categorized in four types: a) elongated tubular morphology; b) elongated tubular morphology with the presence of fragmented mitochondria with round morphology; c) short tubular morphology with the presence of fragmented mitochondria with large round morphology; and d) very fragmented mitochondria with small and round morphology. For this study, categories a) and b) were grouped as Category 1 (Cat 1), since is difficult to separate those morphologies, and category c) was named Category 2 (Cat 2) and category d) was named category 3 (Cat 3). The Mitotracker slips were prepared as described above for the following photosensitization treatments: no PS; 25 µM of PS; 50 µM of PS, irradiated and in the dark. The slips were arranged as described in Figure 19.

Figure 19. The slips were observed by the microscope and the mitochondria morphology were categorized by four different types (figure 20, according to Grohm *et al.* [73]

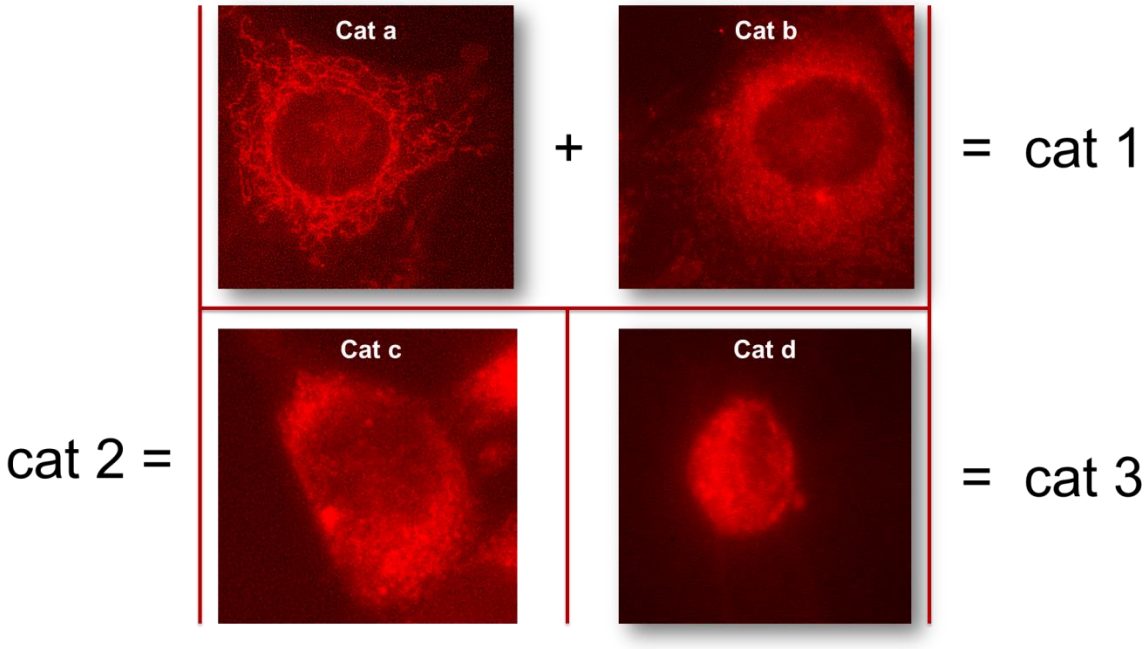

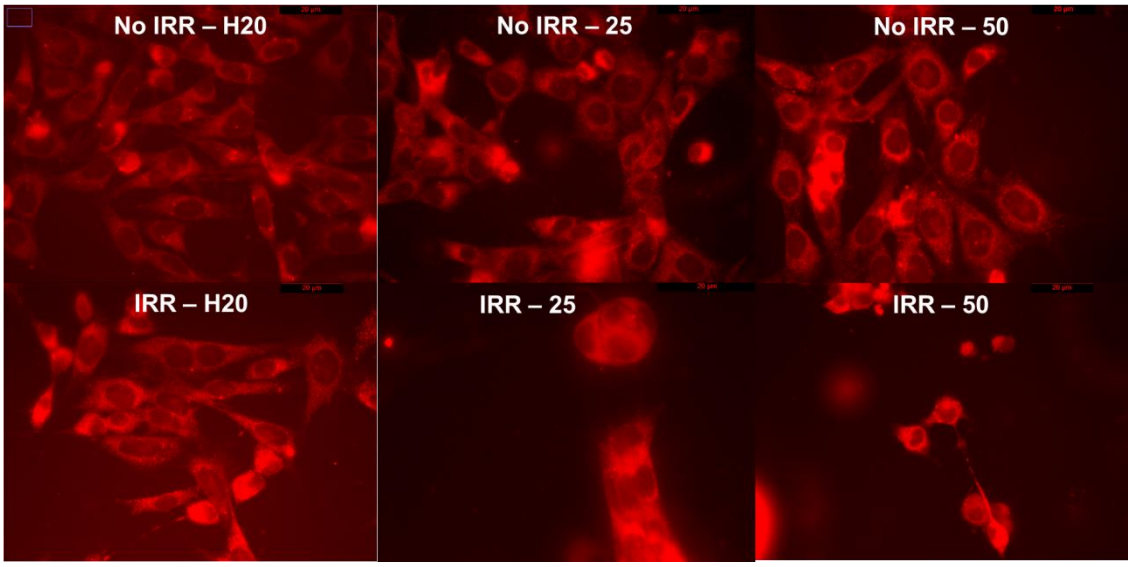

Figure 20. (Above) HT22 cells stained by Mitotracker red, showing typical images of mitochondria categorized in groups 1, 2 and 3. (Below) Untreated HT22 cells stained with Mitotracker red before and after irradiation (No IRR H_2O and IRR H_2O, respectively) and previously treated with with 25 and 50nM of DMMB and irradiated.

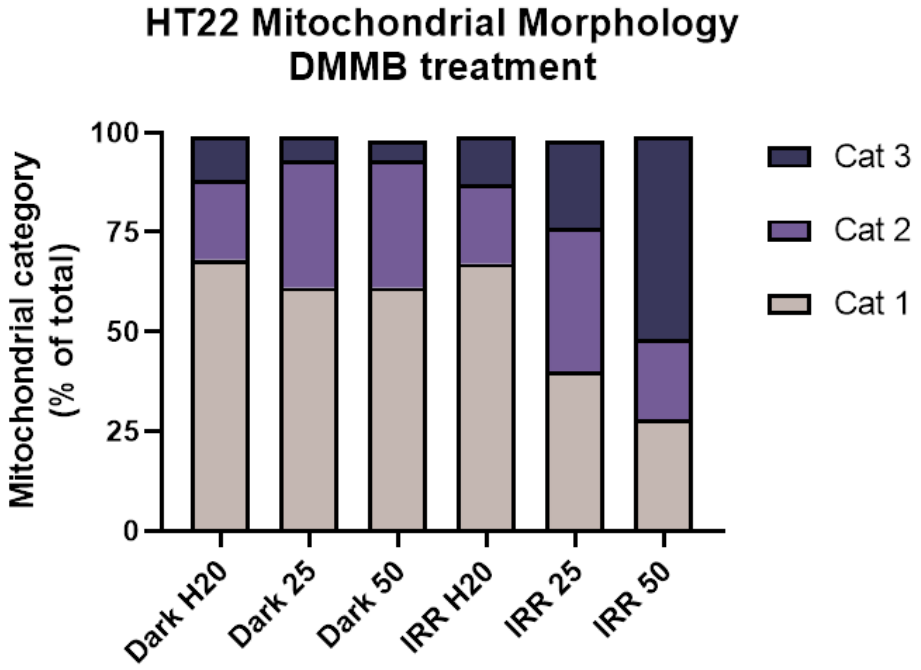

Figure 21. Categorized mitochondria of HT22 cells treated with DMMB and irradiated and dark controls. Average of 250 cell per treatment.

Note in Figure 21 that HT22 cells have a profile distribution of elongated, elongated partially fragmented and fragmented that goes in percent 70:20:10. The sole irradiation in the absence of DMMB does not seem to cause any alteration in the percentage (IRR H_2O). Note however, that the in presence of the photosensitizer (without irradiation) there is already some changes in this distribution. There is a substantial increase in the fraction of mitochondria with elongated partially fragmented population from 20 to 30 percent, with substantial decreases both in the population of intact elongated as well as in the population of highly fragmented mitochondria. This

change can be explained by the fact that DMMB accumulates in mitochondria and, being a phenothiazium cation, it can get involved in mitochondrial electron transfer reactions, even in the dark.[74] Note also that in the presence of DMMB and light the mitochondrial classification in these three populations changes as a function of DMMB concentration. At 25nM, there is a substantial increase in the partially fragmented population, while at 50nM there is a substantial increase in the highly fragmented population, attesting the high level of mitochondrial damage caused by DMMB at this high concentration. It is clear that DMMB is capable of damaging the mitochondria, increasing the category 3 type of morphology, which is indicative of an increase in mitochondria fission.

4. Conclusion and Perspectives

Under proper stimulus of light excitation, DMMB was capable of causing cell death or, in a more precise manner, cause a severe decrease in cell viability. It is possible to observe both increase in the superoxide concentration (MitoSOX staining) and lipid peroxidation (BODIPY) in the treatments with the DMMB. We could not find a proper agent that could protect cells from the photoinduced damage, as it was also the case for cells photosensitized with $Ru(bpy)_3Cl_2$. The efficiency of cell death seems to be higher for DMMB, as LD50 is concentration 1-2 orders of magnitude lower than those observed for the ruthenium complex.

The concentrations used in the assays with DMMB were three orders of magnitude lower (dozens of nanomolars) than those used in the assay with the ruthenium complex (from 25 µM to 50 µM). This is likely to be a consequence of the level of PS internalization as well as the efficiency of membrane binding. Neither of the potential protective agents were capable of protection against the photosensitizers. We aim to continue this work by analysing lipid peroxidation induced by photosensitization of $[Ru(bpy)_3Cl_2]$, and by analysing the subcellular localization of the photosensitizers on the cell line HT22.

5. References

1. Zhang, Q. & Li, L. Photodynamic combinational therapy in cancer treatment. *Journal of B.U.ON.* vol. 23 561–567 (2018).
2. Raquel, D., Almeida, Q. De, Terra, L. F. & Mauri, S. Photodynamic therapy in cancer treatment - an update review. *J. Cancer Metastasis Treat.* 5, 25 (2019).
3. Wu, H., Minamide, T. & Yano, T. Role of photodynamic therapy in the treatment of esophageal cancer. *Dig. Endosc.* 31, 508–516 (2019).
4. El-Hussein, A., Manoto, S. L., Ombinda-Lemboumba, S., Alrowaili, Z. A. & Mthunzi-Kufa, P. A Review of Chemotherapy and Photodynamic Therapy for Lung Cancer Treatment. *Anticancer. Agents Med. Chem.* 21, 149–161 (2020).
5. Zhang, Z. *et al.* An ROS-sensitive tegafur-PpIX-heterodimer- loaded in situ injectable thermosensitive hydrogel for photodynamic therapy combined with chemotherapy to enhance the tegafur-based treatment of breast cancer. *Biomater. Sci.* 9, 221–237 (2020).
6. Yang, H., Liu, R., Xu, Y., Qian, L. & Dai, Z. Photosensitizer Nanoparticles Boost Photodynamic Therapy for Pancreatic Cancer Treatment. *Nano-Micro Lett.* 13, 35 (2021).
7. Deng, X., Shao, Z. & Zhao, Y. Solutions to the Drawbacks of Photothermal and Photodynamic Cancer Therapy. *Adv. Sci.* 2002504, 1–16 (2021).
8. Wang, K., Yu, B. & Pathak, J. L. An update in clinical utilization of photodynamic

therapy for lung cancer. *J. Cancer* 12, 1154–1160 (2021).

9. Ghorbani, J., Rahban, D., Aghamiri, S., Teymouri, A. & Bahador, A. Photosensitizers in antibacterial photodynamic therapy: An overview. *Laser Therapy* vol. 27 1900132 (2018).
10. Lan, M. *et al.* Photosensitizers for Photodynamic Therapy. *Advanced Healthcare Materials* vol. 8 1900132 (2019).
11. Muni, R. H., Altaweel, M., Tennant, M., Weaver, B. & Kertes, P. J. Agreement among canadian retina specialists in the determination of treatment eligibility for photodynamic therapy in age-related macular degeneration. *Retina* 28, 1421–1426 (2008).
12. Biel, M. A. Photodynamic therapy of bacterial and fungal biofilm infections. *Methods Mol. Biol.* 635, 175–194 (2010).
13. Choi, Y. M., Adelzadeh, L. & Wu, J. J. Photodynamic therapy for psoriasis. *J. Dermatolog. Treat.* 26, 202–207 (2015).
14. Bao, L. L. *et al.* In vitro and in vivo evaluation of a pyropheophorbide-a derivative as a potential photosensitizer for age-related macular degeneration. *Biomed. Pharmacother.* 88, 1220–1226 (2017).
15. Zhao, W. *et al.* Topical 5-aminolevulinic acid photodynamic therapy for intra anal-rectal warts. *J. Dermatolog. Treat.* 31, 241–244 (2020).
16. Tehranchinia, Z., Barzkar, N., Mohammad Riahi, S. & Khazan, M. A comparison

of the effects of clobetasol 0.05% and photodynamic therapy using aminolevulinic acid with red light in the treatment of severe nail psoriasis. *J. Lasers Med. Sci.* 11, 3–7 (2020).

17. Zhang, J. *et al.* An updated overview on the development of new photosensitizers for anticancer photodynamic therapy. *Acta Pharmaceutica Sinica B* vol. 8 137–146 (2018).
18. Shokurov, A. V. *et al.* Photosensitized Degradation of Model Lipid Membranes based on 1-palmitoyl-2-oleyl-phosphatidylcholine (POPC). *Prot. Met. Phys. Chem. Surfaces* 54, 19–26 (2018).
19. Srinivas, U. S., Tan, B. W. Q., Vellayappan, B. A. & Jeyasekharan, A. D. ROS and the DNA damage response in cancer. *Redox Biology* vol. 25 101084 (2019).
20. Wu, M. Y. *et al.* Simple synthesis of multifunctional photosensitizers for mitochondrial and bacterial imaging and photodynamic anticancer and antibacterial therapy. *J. Mater. Chem. B* 8, 9035–9042 (2020).
21. Konda, P. *et al.* Discovery of immunogenic cell death-inducing ruthenium-based photosensitizers for anticancer photodynamic therapy. *Oncoimmunology* 10, 1863626 (2021).
22. Baptista, M. S. *et al.* Type I and Type II Photosensitized Oxidation Reactions: Guidelines and Mechanistic Pathways. *Photochemistry and Photobiology* vol. 93 912–919 (2017).

23. Pires, L., Bosco, S. D. M. G., Baptista, M. S. & Kurachi, C. Photodynamic therapy in pythium insidiosum - An in vitro study of the correlation of sensitizer localization and cell death. *PLoS One* 9, 85431 (2014).

24. Girotti, A. W. & Korytowski, W. Nitric Oxide Inhibition of Chain Lipid Peroxidation Initiated by Photodynamic Action in Membrane Environments. *Cell Biochemistry and Biophysics* vol. 78 149–156 (2020).

25. Yalcinkaya, T., Uzilday, B., Ozgur, R., Turkan, I. & Mano, J. Lipid peroxidation-derived reactive carbonyl species (RCS): Their interaction with ROS and cellular redox during environmental stresses. *Environmental and Experimental Botany* vol. 165 139–149 (2019).

26. Bacellar, Isabel O. L.; Oliyeira, Maria C.; Dantas, L. S. ., Costa, Elierge B.; Junqueira, Helena C.; Martins, Waleska K.; Durantini, Andres M.; Cosa, G., Di Mascio, Paolo; Wainwright, Mark; Miotto, R. & Cordeiro, Rodrigo M.; Miyamoto, Sayuri; Baptista, M. S. Photosensitized Membrane Permeabilization Requires Contact-Dependent Reactions between Photosensitizer and Lipids. *J. Am. Chem. Soc.* 140, 9606–9615 (2018).

27. Bacellar, I. O. L. & Baptista, M. S. Mechanisms of Photosensitized Lipid Oxidation and Membrane Permeabilization. *ACS Omega* 4, 21636–21646 (2019).

28. Naik, P. P. *et al.* Secretory clusterin promotes oral cancer cell survival via inhibiting apoptosis by activation of autophagy in AMPK/mTOR/ULK1 dependent pathway.

Life Sci. 264, 118722 (2021).

29. Ou, L. *et al.* The mechanisms of graphene-based materials-induced programmed cell death: A review of apoptosis, autophagy, and programmed necrosis. *International Journal of Nanomedicine* vol. 12 6633–6646 (2017).
30. Berghe, T. Vanden *et al.* Necroptosis, necrosis and secondary necrosis converge on similar cellular disintegration features. *Cell Death Differ.* 17, 922–930 (2010).
31. Elmore, S. Apoptosis: A Review of Programmed Cell Death. *Toxicologic Pathology* vol. 35 495–516 (2007).
32. Riethmüller, M., Burger, N. & Bauer, G. Singlet oxygen treatment of tumor cells triggers extracellular singlet oxygen generation, catalase inactivation and reactivation of intercellular apoptosis-inducing signaling. *Redox Biol.* 6, 157–168 (2015).
33. Mansoori, B. *et al.* Photodynamic therapy for cancer: Role of natural products. *Photodiagnosis and Photodynamic Therapy* vol. 26 395–404 (2019).
34. Senapathy, G. J., George, B. P. & Abrahamse, H. Exploring the Role of Phytochemicals as Potent Natural Photosensitizers in Photodynamic Therapy. *Anticancer. Agents Med. Chem.* 20, 1831–1844 (2020).
35. Tanaka, S. *et al.* Highly Efficient Singlet Oxygen Generation and High Oxidation Resistance Enhanced by Arsole-Polymer-Based Photosensitizer: Application as a Recyclable Photooxidation Catalyst. *Macromolecules* 53, 2006–2013 (2020).

36. Jiang, X. & Dai, Z. Reactive oxygen species in photodynamic therapy. *Kexue Tongbao/Chinese Sci. Bull.* 63, 1783–1802 (2018).

37. Bonnet, S. Why develop photoactivated chemotherapy? *Dalt. Trans.* 47, 10330–10343 (2018).

38. Matsumoto, Y. Toward photochemistry of integrated heterogeneous systems. *J. Chem. Phys.* 137, 091705 (2012).

39. Rosângela Itri, Carlos M. Marques, M. S. B. Shining light on membranes. in *The Giant Vesicle Book, CRC Press.* 15 (2019).

40. Pavani, C., Uchoa, A. F., Oliveira, C. S., Iamamoto, Y. & Baptista, M. S. Effect of zinc insertion and hydrophobicity on the membrane interactions and PDT activity of porphyrin photosensitizers. *Photochem. Photobiol. Sci.* 8, 233–240 (2009).

41. Engelmann, F. M. *et al.* Interaction of cationic meso-porphyrins with liposomes, mitochondria and erythrocytes. *J. Bioenerg. Biomembr.* 39, 175–185 (2007).

42. Caetano, W. *et al.* Photo-Induced Destruction of Giant Vesicles in Methylene Blue Solutions. *Langmuir* 23, 1307–1314 (2007).

43. Martins, W. K. *et al.* Parallel damage in mitochondria and lysosomes is an efficient way to photoinduce cell death. *Autophagy* 15, 259–279 (2019).

44. Lovejoy, K. S. & Lippard, S. J. Non-traditional platinum compounds for improved accumulation, oral bioavailability, and tumor targeting. *Dalt. Trans.* 38, 10651–10659 (2009).

45. Dolmans, D. E. J. G. J., Fukumura, D. & Jain, R. K. Photodynamic therapy for cancer. *Nat. Rev. Cancer* 3, 380–387 (2003).

46. A. Sgambellone, M., David, A., N. Garner, R., R. Dunbar, K. & Turro, C. Cellular Toxicity Induced by the Photorelease of a Caged Bioactive Molecule: Design of a Potential Dual-Action Ru(II) Complex. *J. Am. Chem. Soc.* 135, 11274–11282 (2013).

47. A. Albani, B. *et al.* Marked Improvement in Photoinduced Cell Death by a New Tris-heteroleptic Complex with Dual Action: Singlet Oxygen Sensitization and Ligand Dissociation. *J. Am. Chem. Soc.* 136, 17095–17101 (2014).

48. Sciuto, E. L. *et al.* Photo-physical characterization of fluorophore Ru(bpy)32+ for optical biosensing applications. *Sens. Bio-Sensing Res.* 6, 67–71 (2015).

49. Oliveira, C. S., Turchiello, R., Kowaltowski, A. J., Indig, G. L. & Baptista, M. S. Major determinants of photoinduced cell death: Subcellular localization versus photosensitization efficiency. *Free Radic. Biol. Med.* 51, 824–833 (2011).

50. Abdel-Shafi, A. A., Hassanin, H. A. & Al-Shihry, S. S. Partial charge transfer contribution to the solvent isotope effect and photosensitized generation of singlet oxygen, O2(1Δ g), by substituted ruthenium(II) bipyridyl complexes in aqueous media. *Photochem. Photobiol. Sci.* 13, 1330–1337 (2014).

51. Junqueira, H. C., Severino, D., Dias, L. G., Gugliotti, M. S. & Baptista, M. S. Modulation of methylene blue photochemical properties based on adsorption at

aqueous micelle interfaces. in *Physical Chemistry Chemical Physics* vol. 4 2320–2328 (2002).

52. Bacellar, I. O. L. *et al.* Membrane Damage Efficiency of Phenothiazinium Photosensitizers. *Photochem. Photobiol.* 90, 801–813 (2014).
53. Mertins, O. *et al.* Physical damage on giant vesicles membrane as a result of methylene blue photoirradiation. *Biophys. J.* 106, 162–171 (2014).
54. Tsubone, T. M. *et al.* Cellular compartments challenged by membrane photo-oxidation. *Arch. Biochem. Biophys.* 697, 108665 (2021).
55. Rotenberg, S. *et al.* Extracellular environment as one mediator of blue light-induced mitochondrial suppression. 22, 759–764 (2006).
56. He, W., Cao, R., Huang, B., Wei, X. & Liang, L. Enhanced red fluorescence emissions of [ru(Bpy)3]cl2 in dna complexes. in *Key Engineering Materials* vol. 842 KEM (2020).
57. Zhang, L. *et al.* Discovery of a ruthenium complex for the theranosis of glioma through targeting the mitochondrial DNA with bioinformatic methods. *Int. J. Mol. Sci.* 20, (2019).
58. Puckett, C. A. & Barton, J. K. Methods to explore cellular uptake of ruthenium complexes. *J. Am. Chem. Soc.* 129, 46–47 (2007).
59. Puckett, C. A. & Barton, J. K. Mechanism of Cellular Uptake of a Ruthenium Polypyridyl Complex. *Biochem. 2008,* 47, 11711–11716 (2008).

60. Lee, S. Y., Kim, C. Y. & Nam, T. G. Ruthenium complexes as anticancer agents: A brief history and perspectives. *Drug Design, Development and Therapy* vol. 14 5375–5392 (2020).

61. Karges, J. *et al.* Rationally designed ruthenium complexes for 1- and 2-photon photodynamic therapy. *Nat. Commun.* 11, 3262 (2020).

62. Ryan, R. T. *et al.* Bis-tridentate N-Heterocyclic Carbene Ru(II) Complexes are Promising New Agents for Photodynamic Therapy. *Inorg. Chem.* 59, 8882–8892 (2020).

63. Deng, Z. *et al.* Ruthenium complexes with phenylterpyridine derivatives target cell membrane and trigger death receptors-mediated apoptosis in cancer cells. *Biomaterials* 129, 111–126 (2017).

64. Liang, N. *et al.* Role of mitochondrial calcium uniporter in regulating mitochondrial fission in the cerebral cortexes of living rats. *J. Neural Transm.* 121, 593–600 (2014).

65. Miotto, G. *et al.* Insight into the mechanism of ferroptosis inhibition by ferrostatin-1. *Redox Biol.* 28, 101328 (2020).

66. Pallast, S., Arai, K., Wang, X., Lo, E. H. & Van Leyen, K. 12/15-Lipoxygenase targets neuronal mitochondria under oxidative stress. *J. Neurochem.* 111, 882–889 (2009).

67. Xie, C. *et al.* N-Acetylcysteine reduces ROS-mediated oxidative DNA damage and

PI3K/Akt pathway activation induced by Helicobacter pylori infection. *Oxid. Med. Cell. Longev.* 2018, 1874985 (2018).

68. Zafarullah, M., Li, W. Q., Sylvester, J. & Ahmad, M. Molecular mechanisms of N -acetylcysteine actions. *Cell. Mol. Life Sci.* 60, 6–20 (2003).
69. Sun, S.-Y. N-acetylcysteine, reactive oxygen species and beyond. *Cancer Biol. Ther.* 9, 109–110 (2010).
70. Grzelak, A., Rychlik, B. & Bartosz, G. Light-dependent generation of reactive oxygen species in cell culture media. 30, 1418–1425 (2001).
71. Ryou, M.-G. *et al.* Methylene blue-induced neuronal protective mechanism against hypoxia-reoxygenation stress. *Neuroscience* 301, 193–203 (2015).
72. Martins, W. K. *et al.* Parallel damage in mitochondria and lysosomes is an efficient way to photoinduce cell death. *Autophagy* 15, 259–279 (2019).
73. Grohm, J., Plesnila, N. & Culmsee, C. Bid mediates fission, membrane permeabilization and peri-nuclear accumulation of mitochondria as a prerequisite for oxidative neuronal cell death. *Brain. Behav. Immun.* 24, (2010).
74. Gabrielli, D. *et al.* Binding , Aggregation and Photochemical Properties of Methylene Blue in Mitochondrial Suspensions Binding , Aggregation and Photochemical Properties of Methylene Blue in Mitochondrial Suspensions. *Photochem. Photobiol.* 79, 227–232 (2004).

List of Attachments

Attachment 1

The phenomenon of aggregation is of great importance in photochemistry, because in the case of the formation of dimers, or other aggregates, a change in the internal energy levels of the molecule can occur, forming different excited states. In addition to the possibility of transferring energy and electrons that can affect the formation of excited triplet states, fluorescence emission and singlet oxygen generation. The complexes were dissolved in concentrated NaCl solutions (3 M and 5 M), and in Tris buffer solutions with 50 nm diameter liposomes. The absorption spectra of these complexes were obtained and are shown in figures 1 to 6 below.

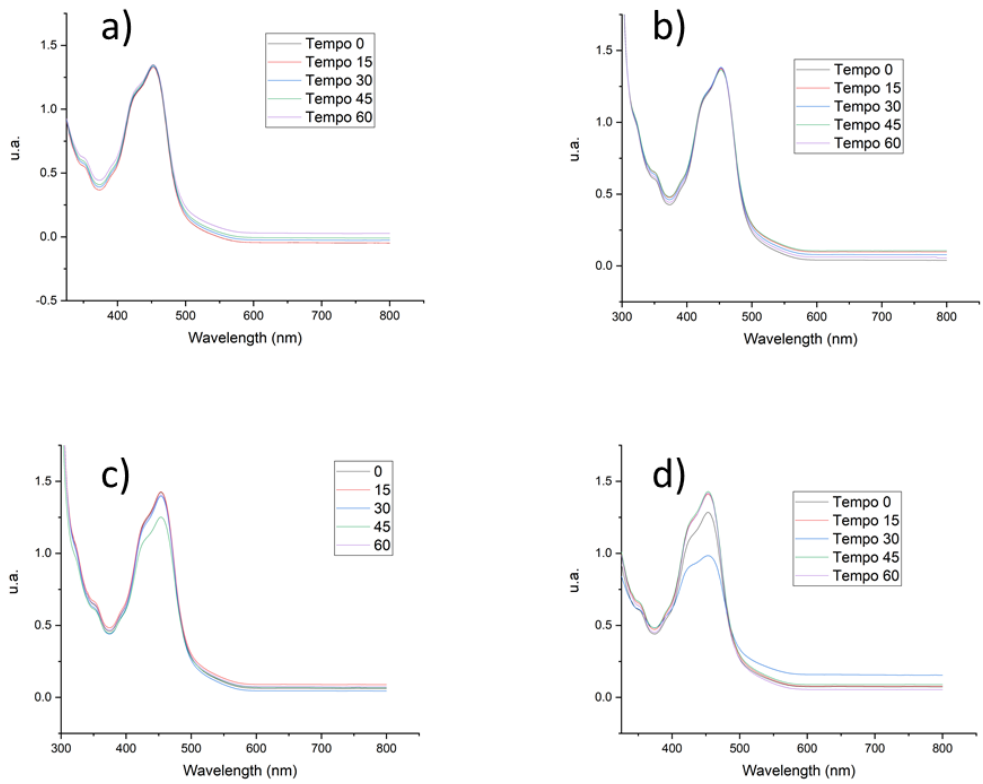

Figure 1. Absorption spectrum of the complex $[Ru(bpy)_3]Cl_2$ at 94 µM. a) In the presence of POPC, b) in the presence of Tris buffer, c) in the presence of NaCl 5 M and d) in the presence of NaCl 3 M.

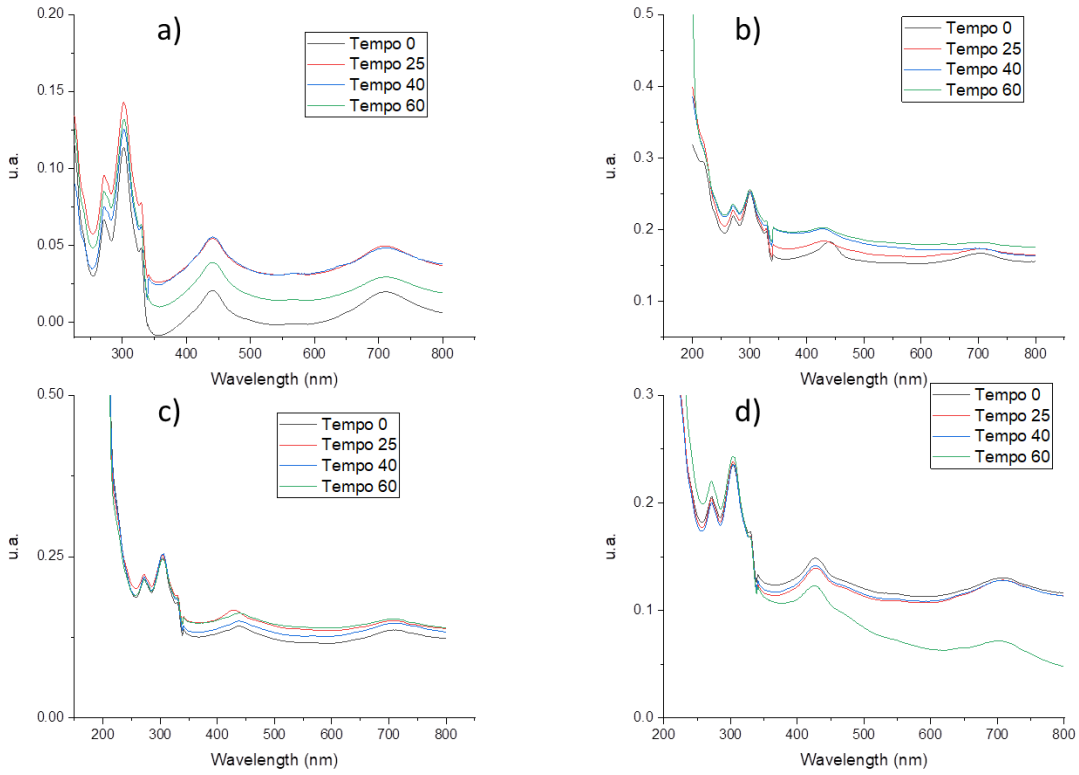

Figure 2. Absorption spectrum of the complex $[Ru(tpy)(ACN)_3]Cl_2$ at 45 µM. a) in the presence of POPC, b) in the presence of Tris buffer, c) in the presence of NaCl 5 M and d) in the presence of NaCl 3M.

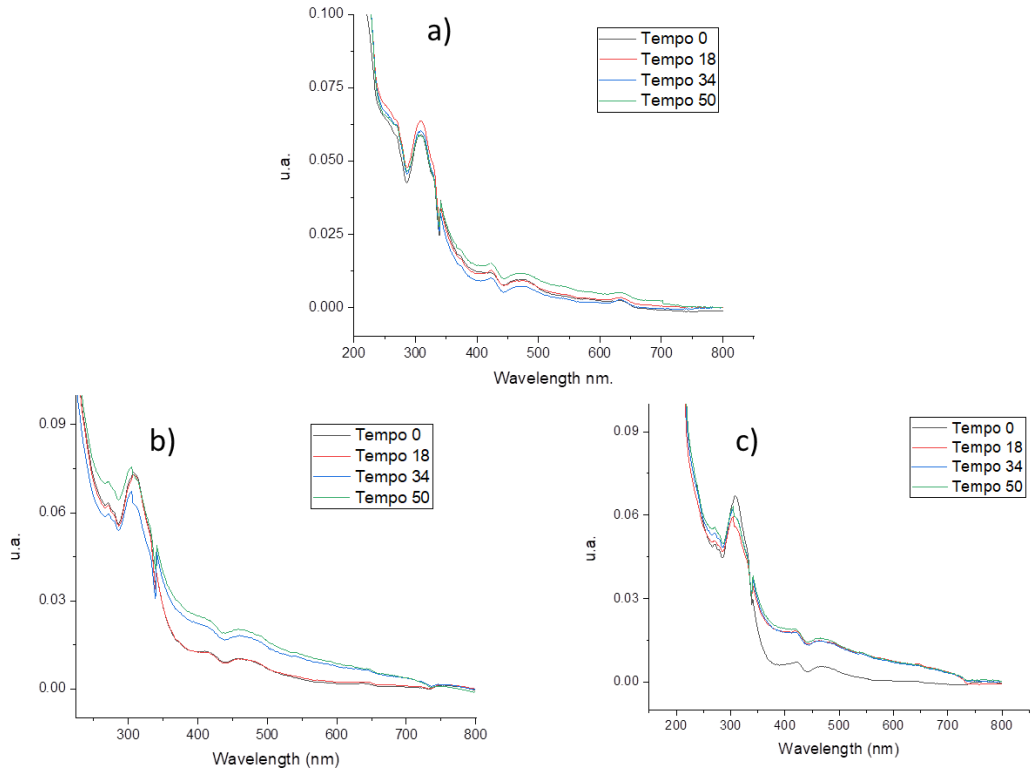

Figure 3. Absorption spectrum of the comples $[Ru(tpy)(5CNU)_3]Cl_2$ at 2.7 µM. a) in the presence of Tris buffer, b) in the presence of NaCl 5 M and c) in the presence of NaCl 3 M.

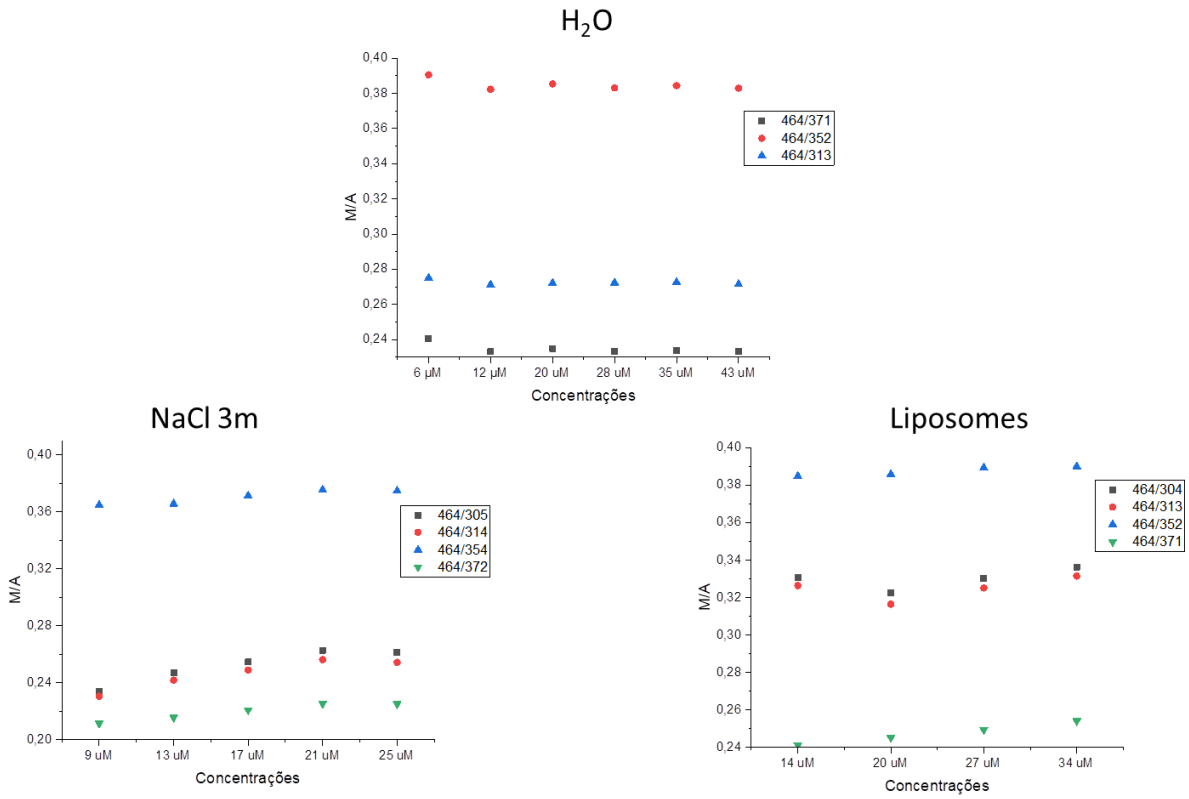

Figure 4. [Ru(dqpy)(phen)(ACN)]$(PF_6)_2$

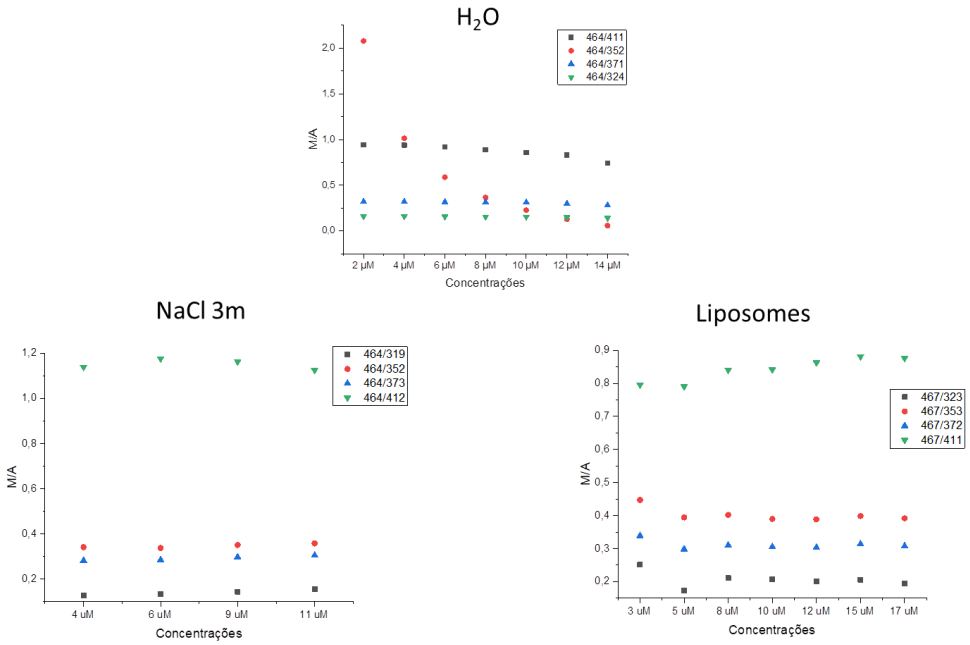

Figure 5. [Ru(dqpy)(dppn)(ACN)]$(PF_6)_2$

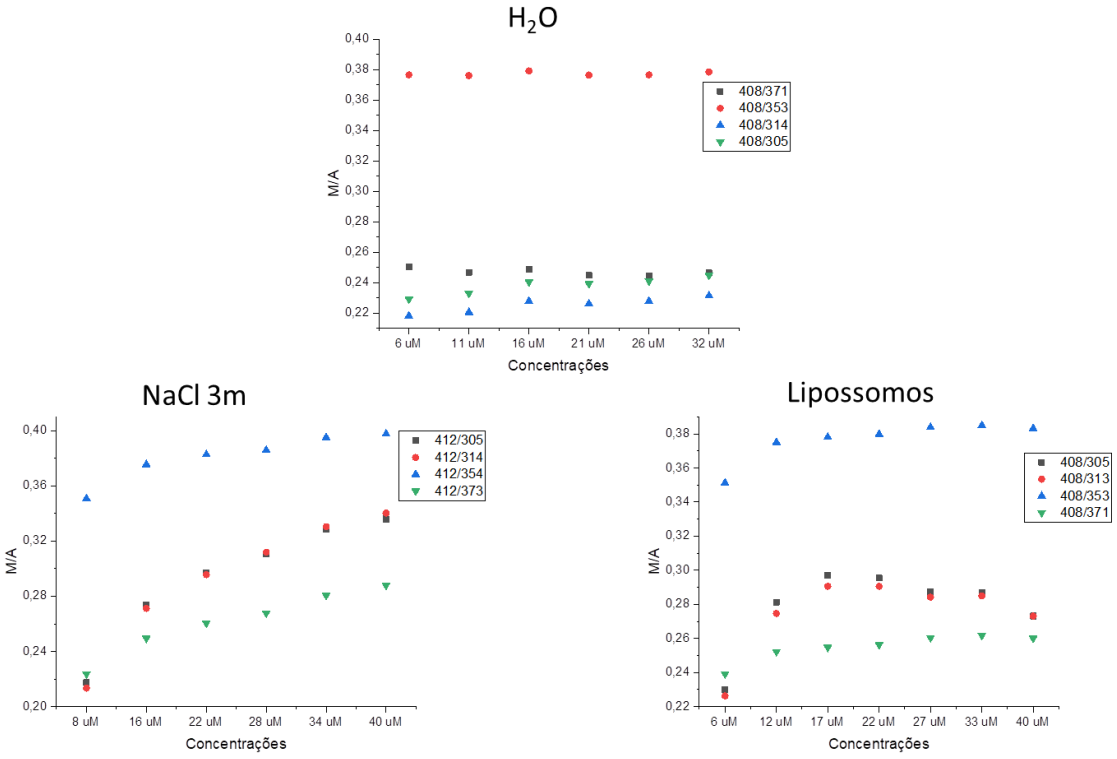

Figure 6. [Ru(dqpy)(phen)(5CNU)]$(PF_6)_2$

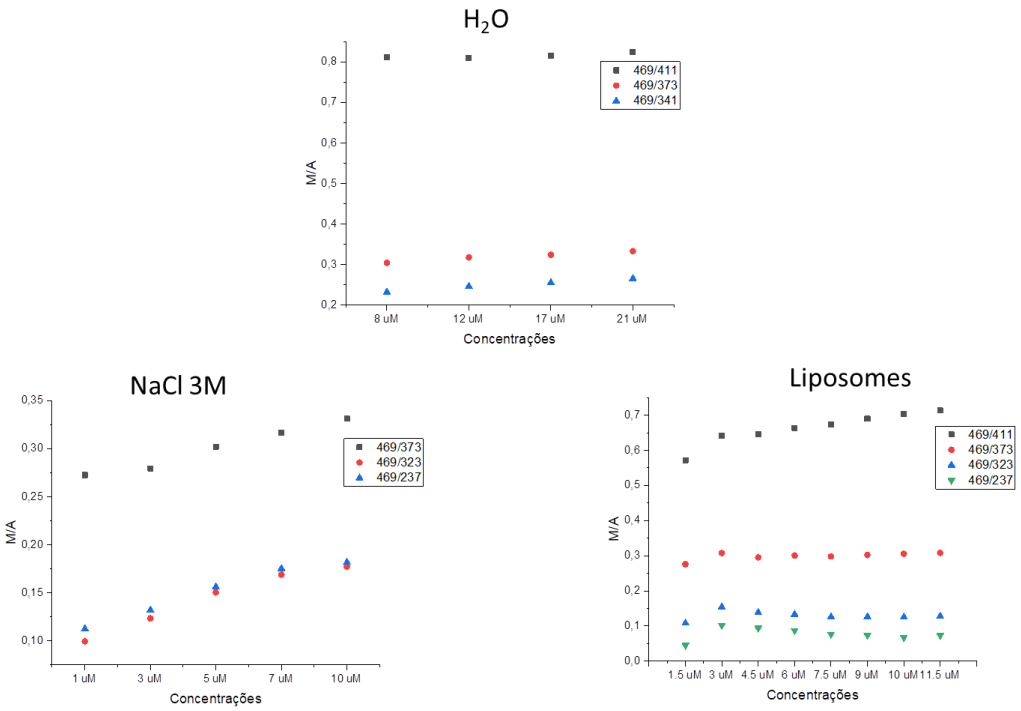

Figure 7. [Ru(dqpy)(dppn)(5CNU)]$(PF_6)_2$

Attachment 2

We describe below the various tries to make the carboxifluorescein test with Ruthenium complexes. Although, we tried many different conditions the quality of the data was never enough to allow quantifications. The main problem is that the probe and the photosensitizers absorb in similar wavelength regions, making it difficult to separate the effects that are due to the photosensitized oxidations to those happening due to direct photochemical events of the probe.

Only the $[Ru(bpy)_3]Cl_2$ complex has been used in these studies, in order to determine optimized experimental conditions before using the other complexes. The complex was tested with a 466 nm led (blue) and a 522 nm led (green). During the tests with the $[Ru(bpy)_3]Cl_2$ complex, experiments with the methylene blue 1,9-dimethyl complex (DMMB) with the 633 nm red led were performed concomitantly, as a positive control. Tests with DMMB have already been carried out previously by the group and showed high membrane permeabilization.[52]

Briefly, in a 96-well microplate with a transparent bottom, 10 µL of a 50 nm diameter liposome solution was added, varying volumes of a stock PS solution, and a sufficient volume of a Tris buffer to complete 200 µL in each well. This microplate was irradiated by a led, and the fluorescence of the wells was observed by a plate reader (for more information, see section 3.5).

The experiments with the DMMB complex were carried out on the Ethik radiator at 633 nm with 11% power (from 1.7 to 2.1 mW cm^{-2}). The tests were performed with Soy Lecithin and POPC liposomes.

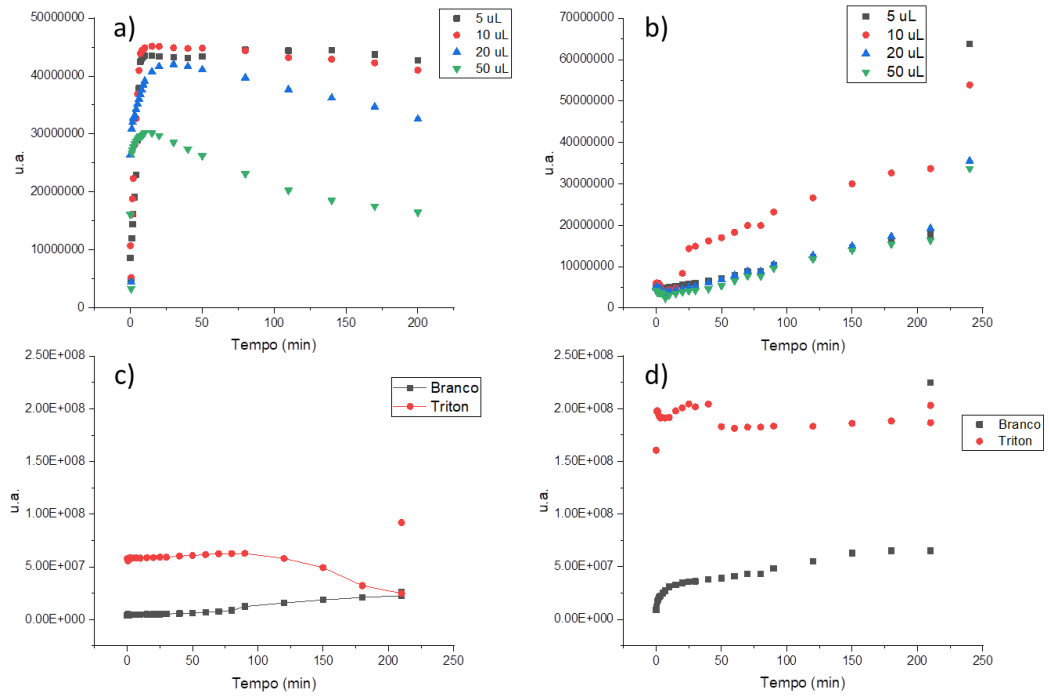

Figure 1. a) fluorescence emisson of CF encapsulated by lipossomes of soy lethicin (a and c) and of POPC (b and d) in the presence of DMMB. The figures c and d shows the controls in the absence of PS, in the triton dots, the lipossomes were blown at the beginning of the experiment.

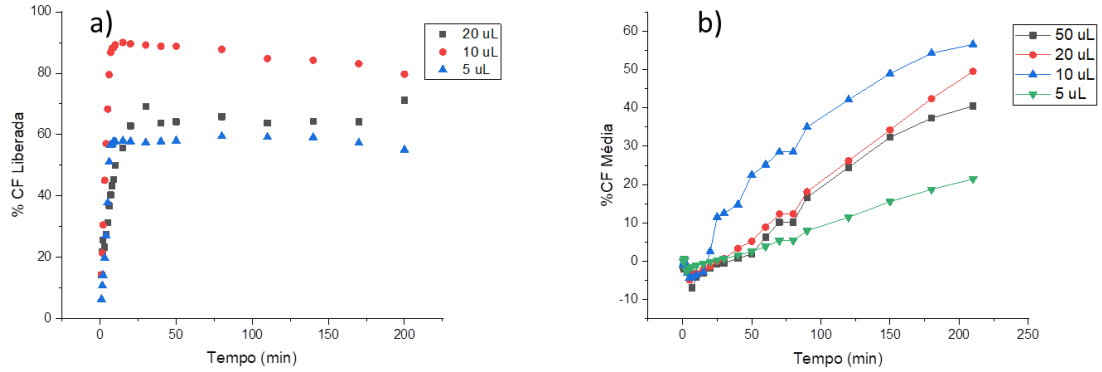

Figure 2. % de CF leaked of the lipossomes of soy lethicin (a) and of POPC (b).

In figure 1 it is possible to observe the fluorescence emission of CF by the irradiation time, in the presence of DMMB and liposomes made of POPC (1a, c) and soy lecithin (1b, d). The emission of CF increases with time, demonstrating a permeabilization of the membrane, from these data the percentages of leaked CF were calculated (as described in section 3.5). Figure 2 shows the percentages of CF leaked as a function of irradiation time. In the case of liposomes made up of POPC, the percentage of leaked CF reached around 60%, and in the case of soy lecithin, around 90%.

A blue led of 466 nm, with power between 1.7 and 2.2 mW cm^{-2} was used to irradiate the microplate. The tests were performed with liposomes of Soy Lecithin, POPC and mixtures of POPC with POPG, in this case in the proportion of 7: 3 (POPC: POPG). The fluorescence of the wells was recalled by obtaining a curve according to figures 2 and 3.

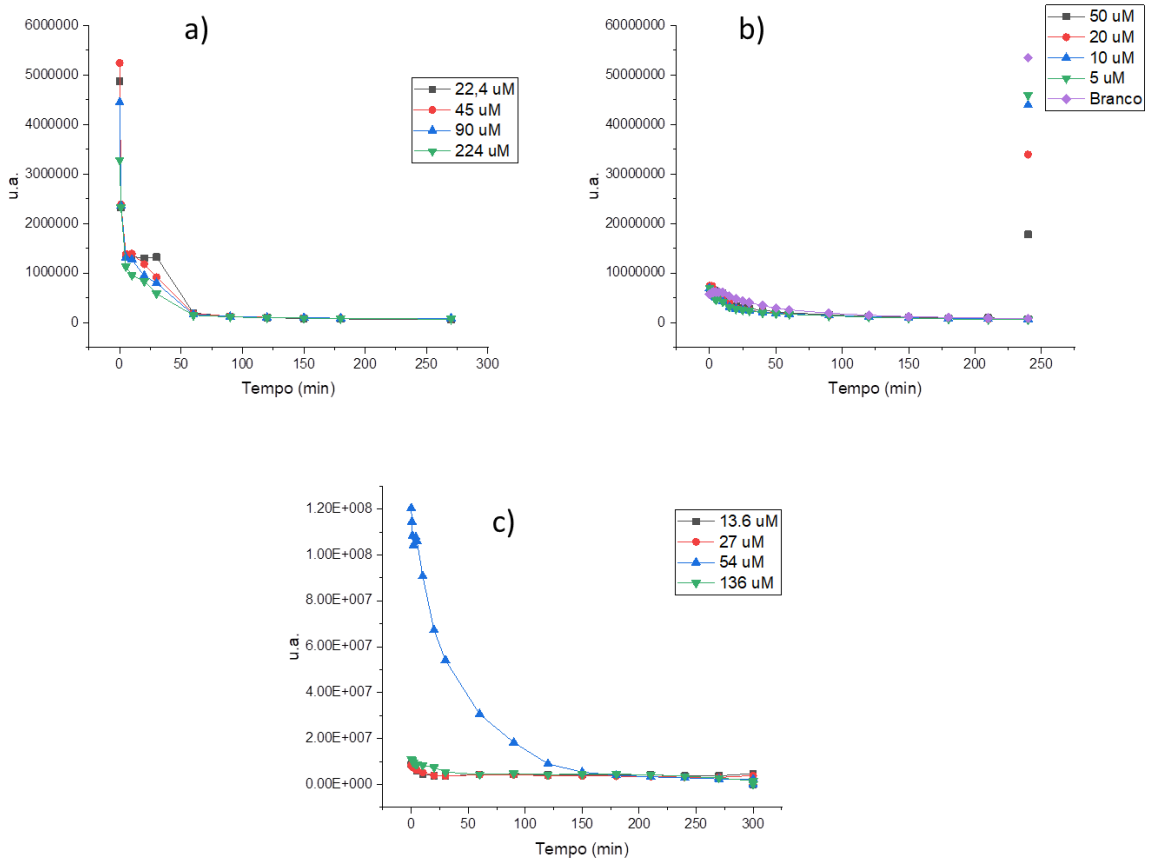

Figure 3. Fluorescence emission of CF encapsulated by lipossomes of soy lethicin (a), POPC (b) and a mixture of 7:3 POPC:POPG (c). The last dot is correspondent to the addition of triton to the wells.

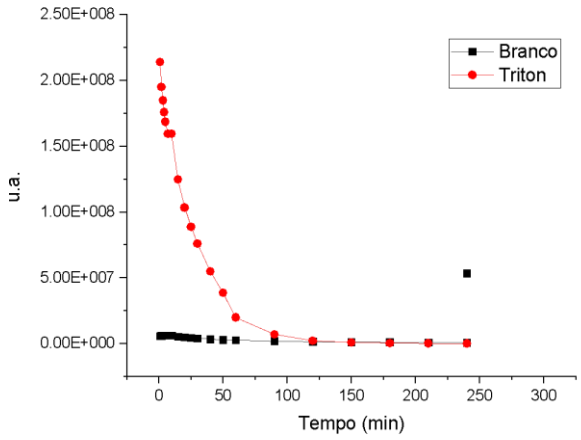

Figure 4. Fluorescence emission of CF encapsulated by POPC liposomes. At the triton dot, the liposomes were blown at the beginning of the experiment.

Figure 3 shows a decrease in the fluorescence emission of FC over time. It was expected that the fluorescence of the wells would increase over time, as the complex would damage the membrane, that is, permeabilize, and allow the leakage of carboxyfluorescein (CF), as demonstrated in the experiments with DMMB. However, it was not possible to calculate the percentage of carboxyfluorescein poured into the medium, since the observed (figure 4) is the decrease in fluorescence over time. In figure 17, it can be seen that the decrease in the fluorescence emission of CF is smaller while it is encapsulated and suppressed in the liposomes. Demonstrating that it undergoes photodegradation when irradiated at that wavelength, and that while it is suppressed in liposomes, this photodegradation is less.

Analysing the decrease in fluorescence in the wells with the complexes and comparing it with the decrease in fluorescence in the white, which contained only lipids and buffer (Figure 4), it is possible to observe that in the wells containing the complex the decrease in fluorescence is more accentuated, and at the end of the experiment, by adding detergent and bursting the liposomes, it is possible to verify a greater photodegradation in the wells that contain the complexes than in the white (figure 5). It can be noted that the higher the concentration of the complex, the greater the photodegradation of CF

In an attempt to avoid the photodegradation of CF, an Ethik irradiator with a green led of 522 nm, 36% power (2.0 to 2.3 mW cm^{-2}) was used. The tests were performed with liposomes of Soy Lecithin, POPC and mixtures of POPC with POPG, in this case in the proportion of 9: 1, 8: 2 and 7: 3 (POPC: POPG). The fluorescence of the wells was recalled by obtaining a curve according to figures 5 and 6.

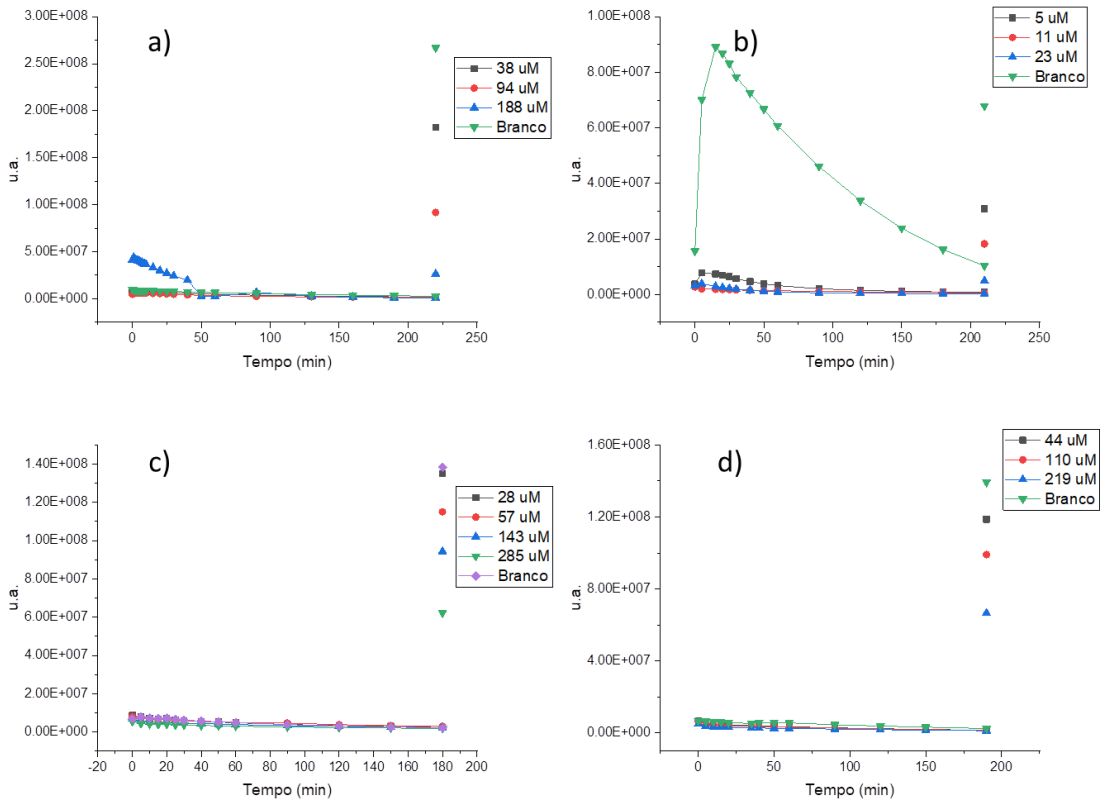

Figure 5. Fluorescence emission of CF encapsulated by liposomes of POPC (a), mixtures of POPC:POPG at the mass proportion of 9:1 (b), 8:2 (c) and 7:3 (d). The last dot is correspondent to the addition of triton to the wells.

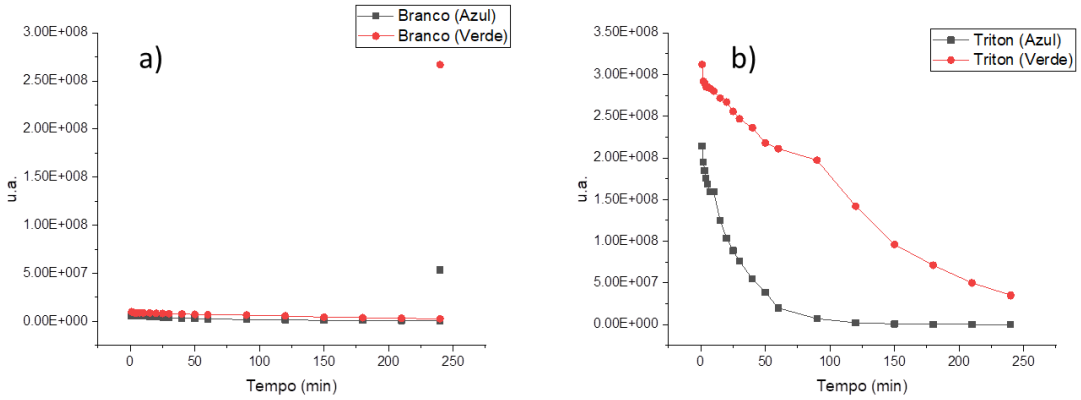

Figure 6. Fluorescence emission of CF encapsulated by liposomes (POPC) by Blue and Green LEDs. At the triton dot, the liposomes were blown at the beginning of the experiment.

Again, a tendency towards photodegradation of FC was observed, however, a lower percentage of degraded FC can be noticed (Figure 6). One possible explanation for this result is that the ruthenium complex could absorb the light emitted by CF fluorescence. Thus, the higher the concentration of the ruthenium complex, the lower the fluorescence emission by CF. However, low concentrations of the ruthenium complex were used, which should not cause such a difference in the results.

Another possible explanation would be if the ruthenium complex participated in the photodegradation of CF. Thus, the ruthenium complex would actively participate in the photodegradation of CF. In this case, even if the ruthenium complex caused a membrane permeabilization, the released CF would only be photodegraded more quickly, which could also explain the results. Still, all cases may have occurred concurrently.